Article

Cell Metabolism

Dietary lipids inhibit mitochondria transfer to macrophages to divert adipocyte-derived mitochondria into the blood

Graphical abstract

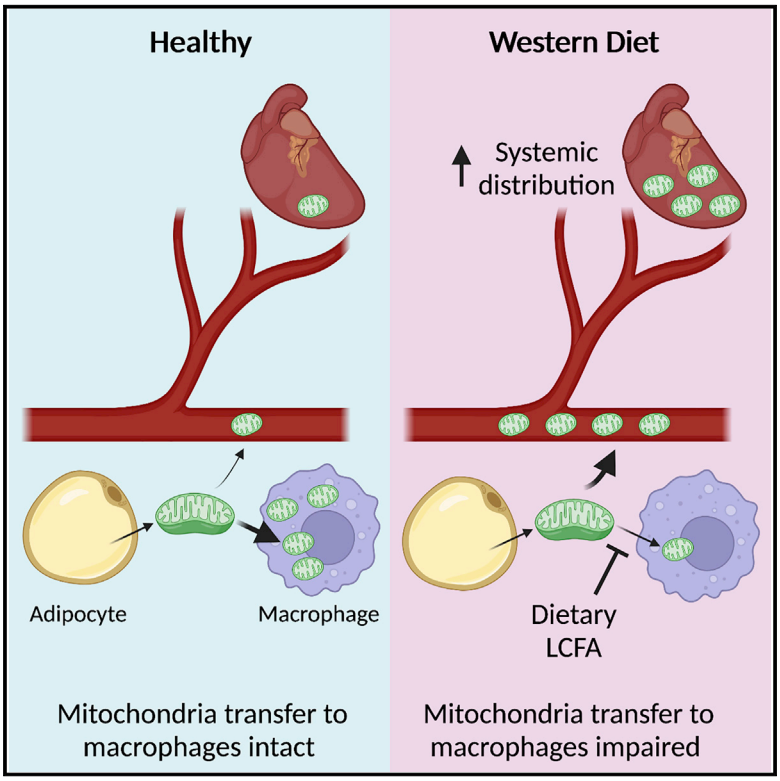

Authors

Nicholas Borcherding, Wentong Jia, Rocky Giwa, ..., Kory Lavine, Clair Crewe, Jonathan R. Brestoff

Correspondence

borcherding.n@wustl.edu (N.B.), brestoff@wustl.edu (J.R.B.)

In brief

Borcherding et al. demonstrate that dietary long-chain fatty acids inhibit intercellular mitochondria transfer from adipocytes to macrophages in white adipose tissue. Inhibiting mitochondria capture by macrophages diverts adipocyte-derived mitochondria into the blood for systemic distribution to distant organs, such as the heart.

Highlights

- Adipocytes transfer mitochondria to tissue-specific networks of cells in fat
- Diet-induced obesity, but not aging, impairs mitochondria transfer to macrophages
- Dietary long-chain fatty acids inhibit mitochondria uptake by macrophages
- Macrophages limit the release of adipocyte mitochondria into blood

Borcherding et al., 2022, Cell Metabolism *34*, 1499–1513
October 4, 2022
https://doi.org/10.1016/j.cmet.2022.08.010

CellPress

Cell Metabolism

CellPress

Article

Dietary lipids inhibit mitochondria transfer to macrophages to divert adipocyte-derived mitochondria into the blood

Nicholas Borcherding,[1,6,*] Wentong Jia,[1,6] Rocky Giwa,[1] Rachael L. Field,[1] John R. Moley,[1] Benjamin J. Kopecky,[2] Mandy M. Chan,[1,2] Bin Q. Yang,[2] Jessica M. Sabio,[3] Emma C. Walker,[4] Omar Osorio,[2] Andrea L. Bredemeyer,[2] Terri Pietka,[2] Jennifer Alexander-Brett,[1,2] Sharon Celeste Morley,[1,4] Maxim N. Artyomov,[1] Nada A. Abumrad,[2,3] Joel Schilling,[1,2] Kory Lavine,[1,2,5] Clair Crewe,[2,3] and Jonathan R. Brestoff[1,7,*]

[1]Department of Pathology and Immunology, Washington University School of Medicine, St Louis, MO 63110, USA
[2]Department of Medicine, Washington University School of Medicine, St Louis, MO 63110, USA
[3]Department of Cell Biology and Physiology, Washington University School of Medicine, St Louis, MO 63110, USA
[4]Department of Pediatrics, Washington University School of Medicine, St Louis, MO 63110, USA
[5]Department of Developmental Biology, Washington University School of Medicine, St Louis, MO 63110, USA
[6]These authors contributed equally
[7]Lead contact
*Correspondence: borcherding.n@wustl.edu (N.B.), brestoff@wustl.edu (J.R.B.)
https://doi.org/10.1016/j.cmet.2022.08.010

SUMMARY

Adipocytes transfer mitochondria to macrophages in white and brown adipose tissues to maintain metabolic homeostasis. In obesity, adipocyte-to-macrophage mitochondria transfer is impaired, and instead, adipocytes release mitochondria into the blood to induce a protective antioxidant response in the heart. We found that adipocyte-to-macrophage mitochondria transfer in white adipose tissue is inhibited in murine obesity elicited by a lard-based high-fat diet, but not a hydrogenated-coconut-oil-based high-fat diet, aging, or a corn-starch diet. The long-chain fatty acids enriched in lard suppress mitochondria capture by macrophages, diverting adipocyte-derived mitochondria into the blood for delivery to other organs, such as the heart. The depletion of macrophages rapidly increased the number of adipocyte-derived mitochondria in the blood. These findings suggest that dietary lipids regulate mitochondria uptake by macrophages locally in white adipose tissue to determine whether adipocyte-derived mitochondria are released into systemic circulation to support the metabolic adaptation of distant organs in response to nutrient stress.

INTRODUCTION

Obesity is an increasingly prevalent metabolic disease and affects more than 42% of adults in the United States (Hales et al., 2020). The expansion of white adipose tissue (WAT) in obesity is characterized by mitochondrial dysfunction in adipocytes and chronic low-grade inflammation in WAT (Hotamisligil, 2017; Sun et al., 2011). Although many innate and adaptive immune cells have been identified in white, beige, and brown fat depots, macrophages have emerged as particularly important regulators of adipose tissue function (Dalmas et al., 2011; Hotamisligil, 2017; Olefsky and Glass, 2010; Wellen and Hotamisligil, 2003). In the lean state, adipose tissue-resident macrophages support the regulation of lipid, glucose, and energy metabolism (Brestoff and Artis, 2015; McNelis and Olefsky, 2014). However, in the context of obesity, pro-inflammatory macrophages accumulate in WAT and directly contribute to metabolic dysfunction in adipocytes and metabolic disease pathogenesis (Hotamisligil, 2017; Lumeng et al., 2008; Lumeng et al., 2007; Makki et al., 2013; Saltiel and Olefsky, 2017). Although it is well established that immune cells can orchestrate metabolic responses in adipose tissues, the mechanisms by which adipocytes and various immune cell populations communicate are not fully understood.

An emerging body of literature indicates that some cells can transfer their mitochondria to other cell types *in vitro* and *in vivo*. Mitochondria can be released from cells as free mitochondria or in extracellular vesicles (EVs), and both of these forms of mitochondria have been reported to circulate in the blood of mice and humans (Al Amir Dache et al., 2020; Boudreau et al., 2014; Crewe et al., 2021; Levoux et al., 2021). Some cell types can engulf released mitochondria to support their metabolic fitness. For example, it has been observed that mitochondria-deficient ρ^0 cells, which lack functional mitochondria, can capture purified mitochondria from supernatants or other cells *in vitro* and utilize these exogenous mitochondria to rescue defects in aerobic respiration and enhance cell division (Chang et al., 2019; Griesinger et al., 2017; Jackson et al., 2016; Kim et al., 2018; Spees et al., 2006). *In vivo*, astrocytes can donate mitochondria to

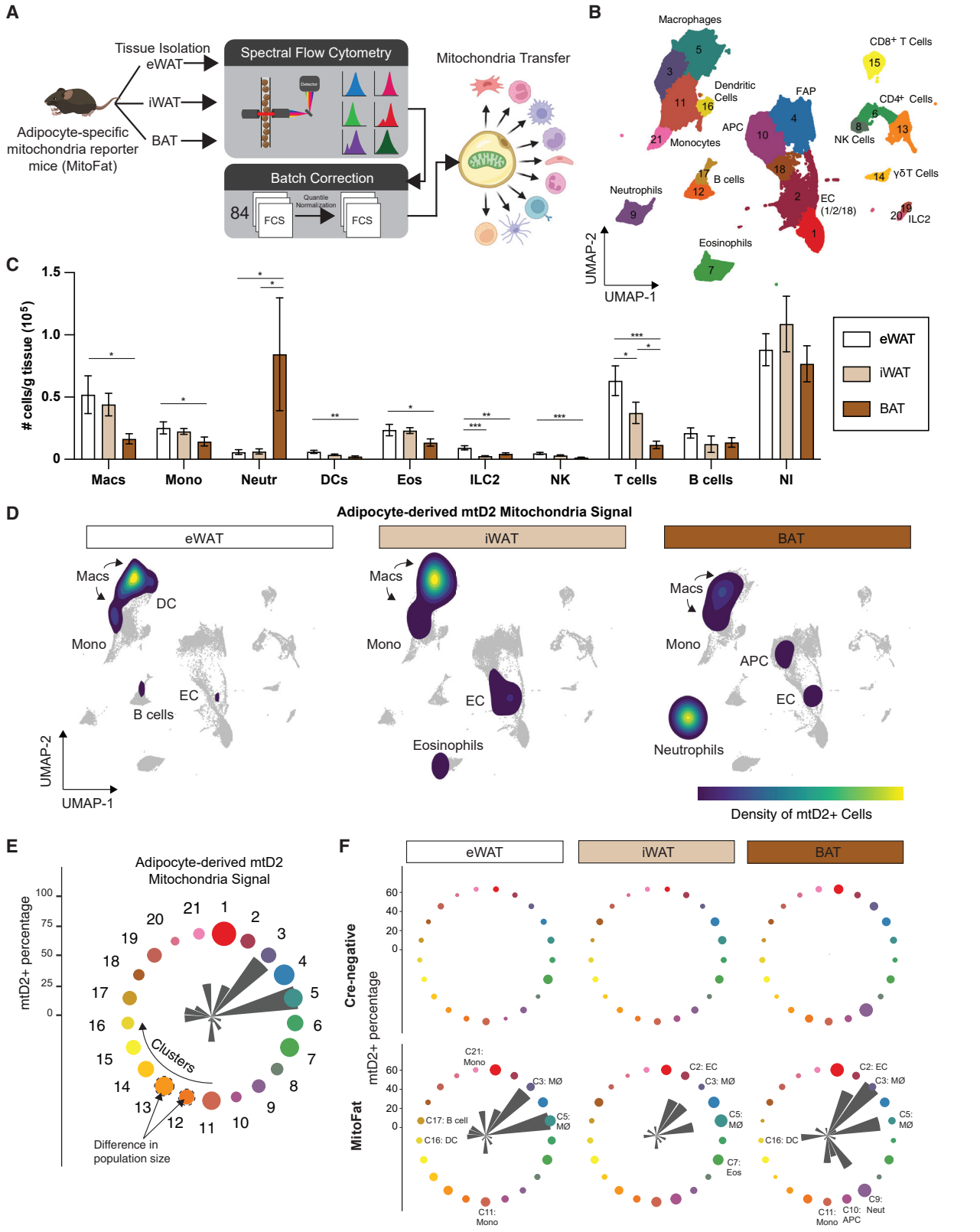

(legend on next page)

neurons in the setting of ischemic stroke to support neuronal survival (Hayakawa et al., 2016), and some cancer cells can capture mitochondria to support tumorigenesis and cell proliferation (Dong et al., 2017; Lu et al., 2017; Rebbeck et al., 2011). Intercellular mitochondria transfer has also been linked to mitochondria quality control in the heart and brain (Evans and Holzbaur, 2020; Nicolás-Ávila et al., 2020), protection from lipopolysaccharide-induced acute lung injury (Islam et al., 2012), platelet activation-associated inflammation and wound healing (Boudreau et al., 2014; Levoux et al., 2021), immune cell activation in response to infection (Mistry et al., 2019), and inflammation following lung transplantation (Scozzi et al., 2019).

Recently, we demonstrated that adipocytes transfer mitochondria to macrophages in WAT *in vivo* at steady state in a heparan sulfate (HS)-mediated process (Brestoff et al., 2021). Genetic disruption of intercellular mitochondria transfer to macrophages by conditional deletion of the HS biosynthesis gene *Ext1* was associated with decreased energy expenditure, accumulation of fat mass on a chow diet, and exacerbated diet-induced obesity in mice. This suggests that intercellular mitochondria transfer may contribute to the regulation of systemic metabolic homeostasis. It has also been shown that in high-fat diet (HFD)-induced obesity, adipocytes release oxidatively damaged mitochondria into the blood in small EVs for delivery to distant organs such as the heart (Crewe et al., 2021). Inter-organ transport of adipocyte-derived mitochondria induces an antioxidant response that metabolically preconditions the heart to defend against cardiometabolic stress. However, the factors that determine whether adipocytes transfer their mitochondria locally to WAT-resident macrophages or systemically to the heart are poorly understood. Here, we show that dietary long-chain fatty acids (LCFAs) directly inhibit mitochondria transfer to tissue-resident macrophages, diverting adipocyte-derived mitochondria into circulation for distribution to distant organs.

RESULTS

Analysis of mitochondria transfer networks

To investigate the diversity of intercellular mitochondria transfer axes from adipocytes to other cell types in white, beige, and brown fat, we performed multidimensional spectral flow cytometry of epididymal WAT (eWAT), inguinal WAT (iWAT), and interscapular brown adipose tissue (BAT) from adipocyte-specific mitochondria reporter (MitoFat) mice and analyzed the data using machine learning (Figure 1A). To ensure consistent clustering across datasets, we included two separate experiments. The first compared young (4 to 5 months old) and aged (22 to 24 months old) MitoFat mice fed a normal chow diet. The second compared young MitoFat mice fed a chow diet, lard-HFD, or hydrogenated coconut oil (HCO)-HFD. After batch correction, a uniformed manifold approximation and projection (UMAP) of singlet live cells was generated (mtD2 excluded).

This analysis produced 21 distinct clusters of cells (Figure 1B) that were defined by marker distribution (Figure S1A; Table S1), including various innate and adaptive immune cell populations and five CD45-negative non-immune cell types. To determine the identities of the non-immune cells, we designed a second panel (Table S2) with a large degree of overlap with the first. Common markers were used in a batch-specific nearest neighbor analysis (Haghverdi et al., 2018) to map clusters from panel 2 to panel 1 (Figure S1B). Panel 2 successfully mapped to each original cluster (Figure S1C) with variable degrees of confidence (Figure S1D). Using cells that were mapped confidently, we defined clusters 1, 2, and 18 as CD31+ CD34+ EpCAM+ endothelial cells (ECs) and clusters 4 and 10 as PDGFR-α (CD140a)+ adipocyte progenitor cells (APCs) (Figures 1B and S1E), with cluster 4 being CD9^{high} fibro-adipogenic progenitors (FAPs) and cluster 10 being CD9^{low} APCs committed to adipogenesis (Marcelin et al., 2017).

We observed tissue-specific differences in the immune cell composition of the three adipose tissue depots at steady state (Figure 1C). An overlay of mtD2-positive cellular density on the UMAP, which reflects both cellular abundance and mtD2+ frequency, suggested that adipocytes transfer mitochondria to various cell types in a tissue-specific manner (Figure 1D). In eWAT and iWAT, macrophage clusters 3 and 5 were the dominant recipients of adipocyte-derived mitochondria. Although macrophages were also prominent recipients of adipocyte-derived mitochondria in BAT, as recently reported (Rosina et al., 2022), neutrophils (cluster 9) were the most abundant mtD2+ cell population overall, given the large number of neutrophils in BAT (Figures 1C and 1D). An EC population (cluster 2) was also a prevalent mtD2+ cell type in iWAT and BAT, and a low frequency of adipogenic APCs (cluster 10) were mtD2+ in BAT.

To visualize the percentage of each cell type that might contain adipocyte-derived mitochondria, we generated "clock-face diagrams" (Figure 1E). Cluster size reflects relative population abundance. Each cluster is annotated with a minute/hour hand defining the percentage of cells that are mtD2+. In eWAT, adipocyte-derived mitochondria transfer was most appreciable in macrophage clusters 3 and 5. There were less prevalent but detectable mitochondria transfer axes from adipocytes to monocytes, dendritic cells, a population of B cells, and EC cluster 2 (EC2) (Figure 1F). In iWAT, macrophage clusters 3 and 5 and EC2 were the

Figure 1. Multidimensional spectral flow cytometry reveals tissue-specific mitochondria transfer axes from adipocytes in white, beige, and brown fat

(A) Experimental design.

(B) UMAP embedding for 384,869 cells randomly sampled, with annotated clustering.

(C) Numbers per gram of the indicated cell types in eWAT, iWAT, and BAT from n = 8 MitoFat mice. Data are expressed as mean ± SEM. One-way ANOVA with LSD post hoc test per cell type. *$p < 0.05$, **$p < 0.01$, and ***$p < 0.001$.

(D) Relative density of mtD2+ cells.

(E) Clock-face diagram showing the degree of mitochondria transfer from adipocytes to each of the 21 clusters. Dot size reflects relative cluster abundance, and the minute/hour hands are the mean percent mtD2+.

(F) Clock-face diagrams parsed by eWAT, iWAT, and BAT.

See also Figure S1 and Tables S1 and S2.

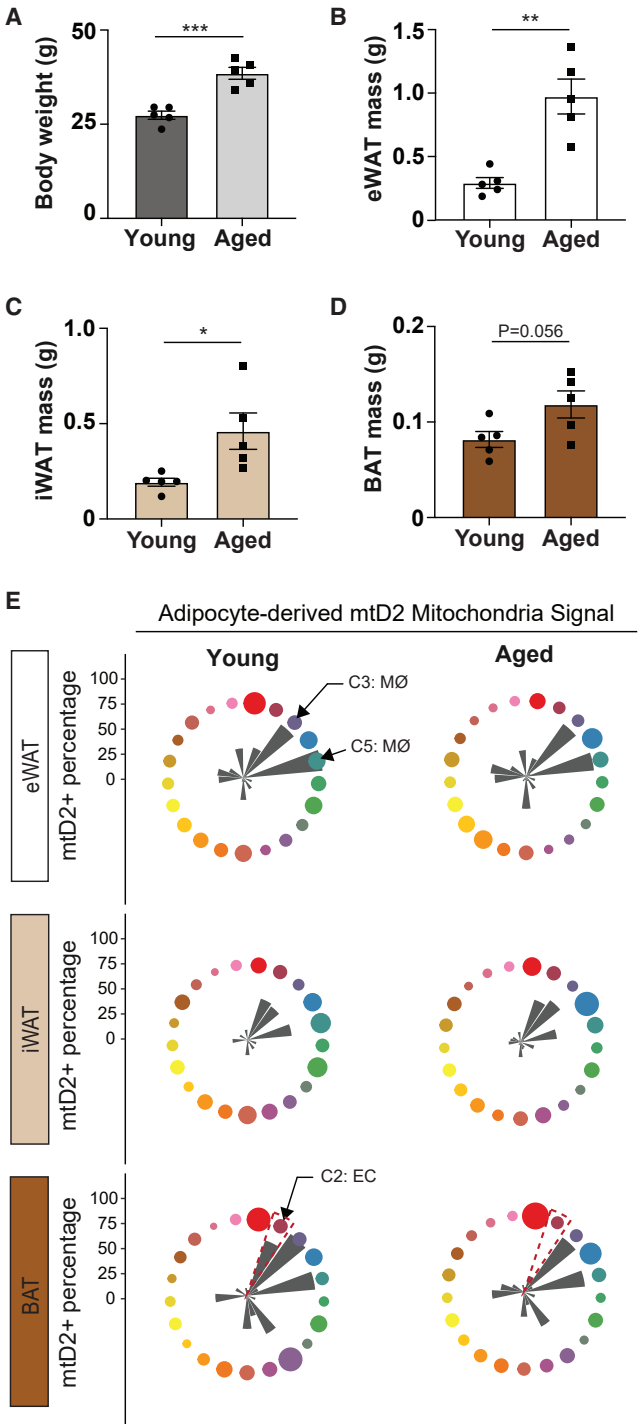

Figure 2. Aging-associated obesity minimally affects mitochondria transfer from adipocytes to other cell types in adipose tissues

(A–D) (A) Body weight and (B) eWAT, (C) iWAT, and (D) BAT masses of young (4 to 5 months old; n = 5) or aged (22 to 24 months old; n = 5) MitoFat mice on a normal chow diet.

(E) Clock-face diagrams comparing mitochondria transfer axes between young and aged MitoFat mice, parsed by eWAT, iWAT, and BAT. Mean ± SEM. Students t tests. *p < 0.05 and **p < 0.01.

See also Figure S2.

dominant mtD2+ cell types. In BAT, adipocyte-to-macrophage mitochondria transfer was also predominant in macrophage clusters 3 and 5, EC2, and neutrophil cluster 9. Less prevalent but detectable mtD2+ cells in BAT included monocyte cluster 11, DCs, and adipogenic APC cluster 10. mtD2+ adipogenic APCs were not detected in eWAT or iWAT, and FAP cluster 4 was not mtD2+ in any of the adipose depots. These findings suggest APCs are not frequent recipients of adipocyte-derived under steady-state conditions, especially in WAT. Collectively, these data suggest there are tissue-specific networks of mitochondria transfer from adipocytes to other cell types in eWAT, iWAT, and BAT but that macrophages are dominant recipients of adipocyte-derived mitochondria across these tissues.

Effect of aging and HFD on mitochondria transfer networks in adipose tissue

To investigate how the network of mitochondria transfer axes originating from adipocytes is altered in aging, we compared 22- to 24-month-old MitoFat mice (Aged) and 4- to 5-month-old MitoFat controls (Young). Aged MitoFat mice weighed more than young mice (Figure 2A) and had increased eWAT, iWAT, and BAT masses (Figures 2B–2D). Histologic analyses indicated that aging was associated with increased adipocyte size in eWAT, iWAT, and BAT and whitening of iWAT and BAT (Figure S2A). Aging was also associated with vascular rarefaction of all three adipose depots (Figure S2B). Cleaved Caspase-3, an indicator of apoptotic cell death in obese adipose tissue (Alkhouri et al., 2010), was also increased in eWAT, iWAT, and BAT from aged mice (Figure S2C).

Despite the marked accumulation of fat mass and the morphologic changes in adipose in aged mice, surprisingly, we did not observe impaired mitochondria transfer from adipocytes to macrophages in eWAT, iWAT, or BAT with aging (Figure 2E). The only mitochondria transfer axis that appeared to be substantially altered in aged MitoFat mice was a reduction in mitochondria transfer from adipocytes to EC2 in BAT (Figure 2E). Previous studies indicate that HS (Brestoff et al., 2021) and CD36 (Rosina et al., 2022) mediate mitochondria uptake by macrophages. We found that expression of HS was reduced in EC2 in eWAT and BAT of aged (19 months old) versus young (4 months old) MitoFat mice (Figure S2D). CD36 expression was also reduced in EC2 in aged eWAT, but not in BAT (Figure S2E). These data indicate that aging-associated obesity is not associated with marked shifts in the network of intercellular mitochondria transfer from adipocytes to immune cells such as macrophages in white, beige, or brown fat.

Considering that aged mice are obese but do not exhibit the same phenotype as young mice fed a HFD (Brestoff et al., 2021), we hypothesized that a dietary factor present in the HFD might impair intercellular mitochondria transfer. To test this, we compared the network of mitochondria transfer axes from adipocytes with other cell types in eWAT, iWAT, and BAT of mice fed a normal chow diet, a lard-HFD (predominantly palmitate, stearate, oleate, and linoleate), or HCO-HFD (predominantly laurate and myristate; Figure S3A). Consistent with prior reports (Stott and Marino, 2020; Wang et al., 2017), mice fed a lard-HFD or HCO-HFD were heavier (Figure 3A) and accumulated more eWAT, iWAT, and BAT mass than mice fed a chow diet (Figures 3B–3D), but body and fat masses were significantly

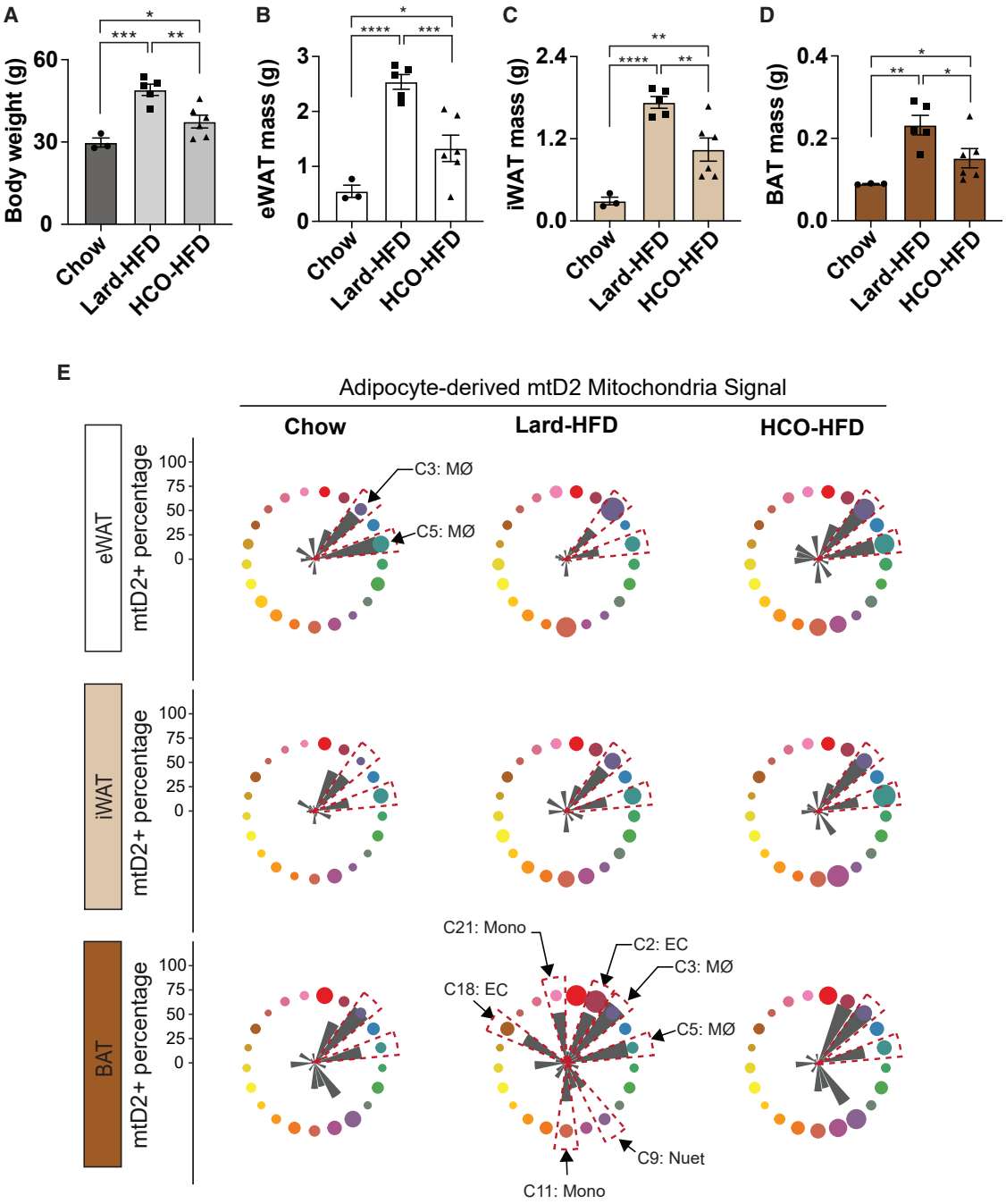

Figure 3. Dietary lipids inhibit mitochondria transfer from adipocytes to macrophages in WAT

(A–D) (A) Body weight and (B) eWAT, (C) iWAT, and (D) BAT masses of young MitoFat mice fed a chow (n = 3), lard-based high-fat diet (HFD; n = 5), or hydrogenated coconut oil (HCO)-based HFD (n = 6) for 9 weeks.

(E) Clock-face diagrams comparing mitochondria transfer axes among the three groups, parsed by eWAT, iWAT, and BAT. Mean ± SEM. One-way ANOVA with Tukey's post hoc test. *p < 0.05, **p < 0.01, ***p < 0.001, and ****p < 0.0001.

See also Figure S3.

lower with the HCO-HFD than lard-HFD. For both lard-HFD and HCO-HFD, histologic analyses demonstrated increased adipocyte size in eWAT, iWAT, and BAT and whitening of iWAT and BAT compared with chow controls (Figure S3B). The two diets had similar effects on adipose vascular rarefaction (Figure S3C), as is known to occur in obese adipose (Shimizu et al., 2014). In contrast, cleaved caspase-3 was markedly higher in lard-HFD eWAT and iWAT than in the HCO-HFD and chow-fed mice (Figure S3D), suggesting that the degree of apoptotic cell death may be elevated with a lard-HFD, but not HCO-HFD.

In eWAT, the lard-HFD was associated with a global contraction in mitochondria transfer from adipocytes, most notably to macrophage clusters 3 and 5 (Figure 3E). However, the HCO-HFD did not result in reductions in any of the mitochondria transfer axes that originated from adipocytes in eWAT, including to macrophage clusters 3 and 5, compared with chow-fed controls. In iWAT, the networks of mitochondria transfer axes had similar patterns in MitoFat mice fed a lard-HFD or HCO-HFD, although it appeared that for both HFDs, there were slight increases in mitochondria transfer to macrophage cluster 3, monocyte cluster 21, and dendritic cells as well as slightly decreased mitochondria transfer to EC cluster 2. In stark contrast to eWAT, in BAT, several mitochondria transfer axes were induced with lard-HFD feeding, including from adipocytes to EC clusters 2 and 18, macrophage clusters 3 and 5, and monocyte clusters 11 and 21. Neutrophils in BAT appeared to have reduced mitochondria transfer from adipocytes with a lard-HFD. These changes were not apparent in BAT of mice fed an HCO-HFD. Collectively, these data suggest that dietary lipids may have tissue-specific effects on intercellular mitochondria transfer axes, with lard-HFD impairing mitochondria transfer in eWAT but inducing mitochondria transfer in BAT.

To account for differences in obesity severity with lard-HFD and HCO-HFD, we performed a weight-matched comparison. We pooled n = 6 chow, n = 6 lard-HFD, and n = 6 HCO-HFD MitoFat mice from 2 separate cohorts, with the goal of establishing lard-HFD and HCO-HFD groups with similar body weights ($p = 0.276$; Figure S3E). In eWAT, a lard-HFD, but not HCO-HFD, was associated with decreased mitochondria transfer from adipocytes to macrophages (Figure S3F). In iWAT, no significant differences were observed across the three diets. In BAT, there was a significant increase in mitochondria transfer from brown adipocytes to macrophages in lard-HFD mice, but not in weight-matched HCO-HFD mice. These data suggest that the differences in adipocyte-to-macrophage mitochondria transfer observed between lard-HFD and HCO-HFD are not due to differential weight gain.

Next, we compared levels of both HS and CD36 on each cluster. Macrophage clusters 3 and 5 in eWAT from lard-HFD MitoFat mice had lower levels of HS (Figure S3G) and CD36 (Figure S3H) than corresponding clusters on a chow diet. These effects were partially or fully restored in eWAT macrophages in mice fed an HCO-HFD. In iWAT macrophages, where adipocyte-to-macrophage mitochondria transfer is not appreciably altered, there were minimal-to-no changes in HS or CD36 expression levels across the three diets. In contrast, in BAT, CD36, but not HS, appeared to be upregulated on macrophages from mice fed a lard-HFD, but not HCO-HFD, reflecting a similar pattern that was observed for mitochondria transfer to macrophages. These data suggest that macrophage expression of HS and CD36, which mediate mitochondria transfer to macrophages in adipose (Brestoff et al., 2021; Rosina et al., 2022), may be regulated by diet.

LCFAs inhibit mitochondria uptake by macrophages

LCFAs such as palmitate induce a pro-inflammatory phenotype in WAT-resident macrophages (Coats et al., 2017; Kratz et al., 2014). Therefore, we initially tested whether palmitate was sufficient to impair mitochondria uptake by macrophage-like BV2 cells. We treated BV2 cells with bovine serum albumin (BSA) (125 μM) or BSA conjugated with palmitate (500 μM), which is equivalent to ~11 nM of free unbound palmitate (Table S3) (Spector et al., 1971; Huber et al., 2006; Zhu et al., 2018) and is similar to the palmitate:BSA ratio of 4:1 seen in HFD-induced obese mice (Yamato et al., 2007). We found that palmitate decreased the percentage of BV2 cells that took up purified mitochondria (Figures 4A and 4B). The increased side scatter-area (SSC-A) in palmitate-treated cells may be due to increased light scattering from the intracellular lipids. In addition, of the cells that had taken up mtD2 mitochondria, the mtD2 mean fluorescence intensity (MFI) was decreased with palmitate treatment, indicating that the biomass of captured mitochondria per cell was also reduced (Figure 4C). Next, we tested whether the other fatty acids prevalent in the lard-HFD and HCO-HFD affect mitochondria uptake by BV2 cells. The LCFAs palmitate, stearate, oleate, and linoleate were sufficient to impair mitochondria uptake by BV2 cells compared (Figure 4D). In contrast, the MCFA laurate appeared to increase the efficiency of mitochondria.

CD36 can bind to palmitate and other LCFAs (Martin et al., 2011; Pepino et al., 2014), and a recent study indicated that CD36 mediates mitochondria capture by macrophages in BAT (Rosina et al., 2022). Therefore, we hypothesized that CD36 might mediate the effects of the LCFAs on mitochondria uptake. The overall degree of mitochondria uptake was significantly lower in CD36-deficient bone-marrow-derived macrophages (BMDMs) than wild-type controls. However, palmitate significantly reduced mitochondria uptake in both $Cd36^{+/+}$ and $Cd36^{-/-}$ BMDMS (Figure 4E). This indicates that CD36 may have a role in mediating mitochondria uptake by macrophages but is not required for palmitate to impair mitochondria uptake. Next, we tested whether palmitate's effect on mitochondria uptake depends on HS. Strikingly, we found that palmitate significantly decreased mitochondria uptake in $Ext1^{+/+}$, but not $Ext1^{-/-}$ BV2 cells, the latter of which cannot make HS (Brestoff et al., 2021; Busse et al., 2007; Figure 4F). This observation indicates that HS are required for palmitate to reduce the ability of macrophages to take up exogenous mitochondria, at least *in vitro*.

To test whether other dietary factors such as common dietary sugars can affect mitochondria capture, we cultured BV2 cells with glucose or sucrose at low or high concentrations. We found that switching from glucose to sucrose had no effect on mitochondria capture by BV2 cells *in vitro* nor did culturing cells with low glucose or low sucrose (Figure 4G). We also fed MitoFat mice 10% kcal fat diets in which the carbohydrate sources were mostly from corn starch or sucrose. Mice fed a corn-starch diet gained more body weight (Figure 4H) and fat mass (Figure 4I) than mice fed a high-sucrose diet; however, the degree of adipocyte-to-macrophage mitochondria transfer did not differ between the two diets for eWAT, iWAT, or BAT (Figure 4J). These data suggest that the dietary carbohydrates sucrose and corn starch do not prominently affect mitochondria transfer from adipocytes to macrophages.

Mitochondria transfer contributes to the metabolic fitness of macrophages

Previous studies indicate the ρ^0 cells, which lack fully functional mitochondria, can capture exogenous mitochondria to restore aerobic respiration (Kim et al., 2018; Spees et al., 2006). To

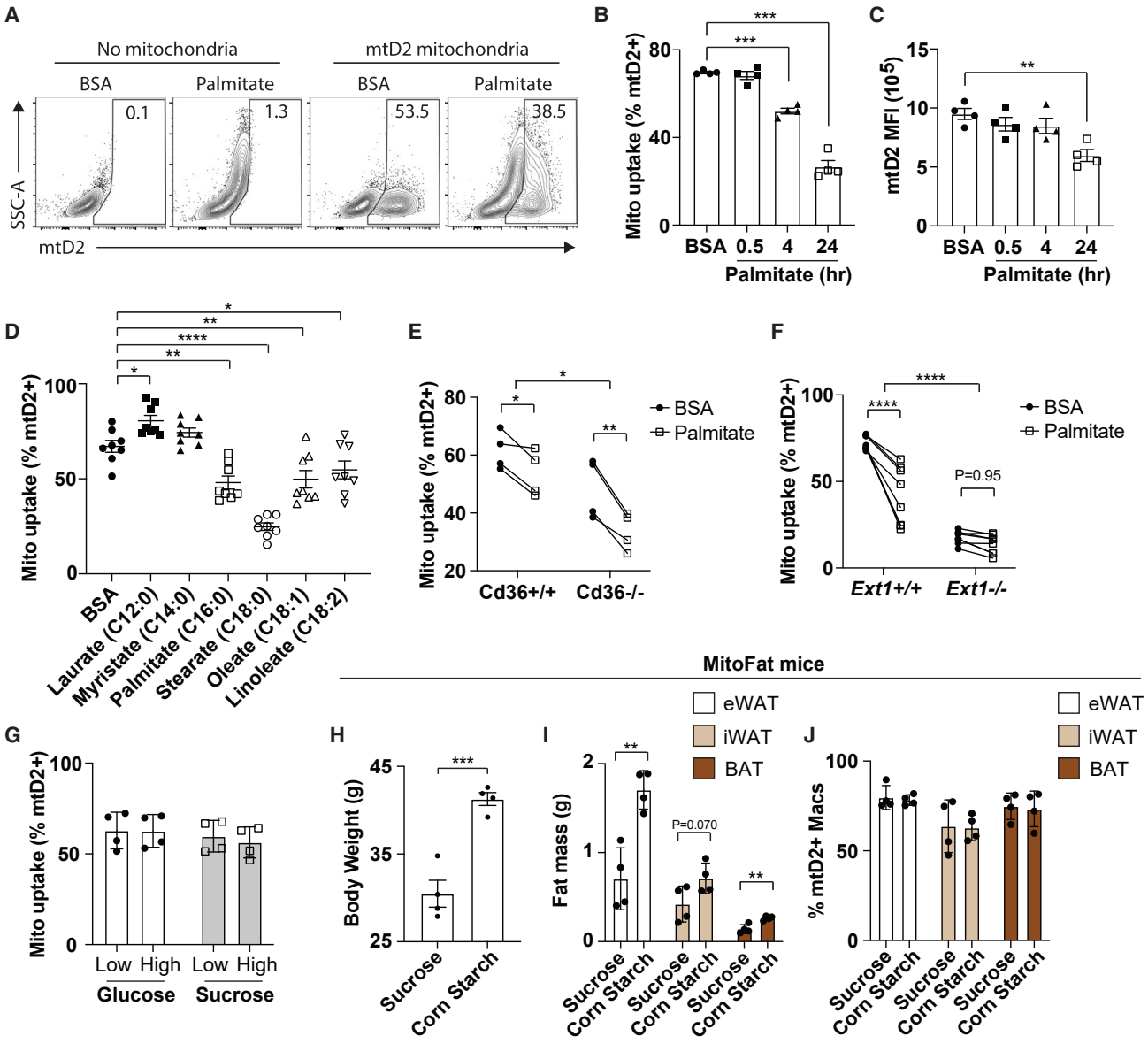

Figure 4. Long-chain fatty acids impair mitochondria uptake *in vitro* in a heparan-sulfate-dependent manner

(A) Flow cytometry plots of BV2 cells treated with BSA or palmitate:BSA for 24 h followed by exposure to mtD2+ mitochondria.

(B and C) (B) Percent mtD2+ and (C) mtD2 MFI (of mtD2+ cells) of BV2 cells treated with BSA for 24 h or 4:1 palmitate:BSA for 0.5, 4, or 24 h. n = 4/group.

(D) Mitochondria uptake by BV2 cells treated with BSA or the indicated BSA-conjugated fatty acids (all 11 nM unbound free fatty acids) for 24 h. N = 8/group.

(E and F) (E) Mitochondria uptake in WT (n = 4) or CD36 KO (n = 4) bone-marrow-derived macrophages or (F) WT (n = 8) or EXT1 KO (n = 8) BV2 cells treated with BSA or 4:1 palmitate:BSA for 24 h.

(G) Mitochondria uptake by BV2 cells cultured with low or high glucose or sucrose for 24 h.

(H–J) (H) Body weights, (I) fat masses, and (J) mitochondria transfer from adipocytes to macrophages in eWAT, iWAT, and BAT in MitoFat mice fed high-sucrose (n = 4) or corn-starch (n = 4) diets for 12 weeks.

For (B)–(D), one-way ANOVA with Holm-Sidak post hoc test against BSA control. For (E)–(G), two-way ANOVA with Sidak post hoc test. For (H)–(J), Student's t tests. Mean ± SEM. *p < 0.05, **p < 0.01, ***p < 0.001, and ****p < 0.0001.

See also Table S3.

determine whether mitochondria transfer affects the mitochondrial metabolism of macrophages in WAT, we performed Seahorse mitochondria stress tests on purified F4/80$^+$ macrophages from ovarian (o)WAT from *Ext1*$^{F/F}$ and *Ext1*$^{\Delta Lyz2}$ mice, the latter of which is known to have impaired mitochondria capture efficiency (Brestoff et al., 2021). We found that *Ext1*$^{\Delta Lyz2}$ oWAT macrophages had similar oxygen consumption rates (OCR) throughout the assay (Figure 5A). Basal, maximal, and ATP production-linked respiration did not differ between groups nor did spare mitochondrial capacity, proton leak, or non-mitochondrial respiration (Figure 5B). Coupling efficiency also did not differ (Figure 5C). These data suggest that under steady-state conditions, HS-mediated

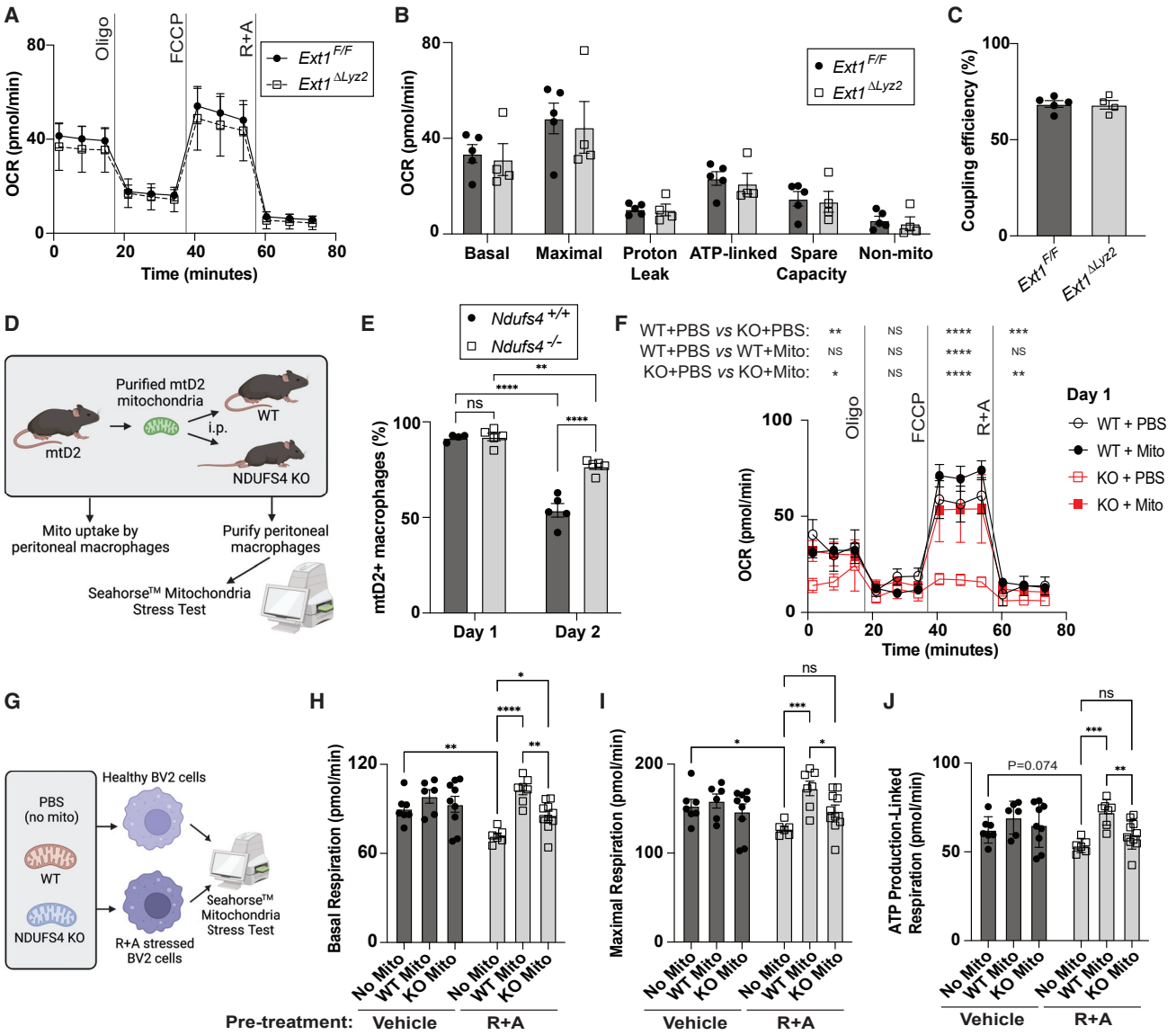

Figure 5. Mitochondria transfer is not required for WAT macrophage mitochondrial metabolism but can restore aerobic respiration in metabolically compromised macrophages

(A–C) (A) Oxygen consumption rates (OCR), (B) mitochondrial metabolism parameters, and (C) coupling efficiency of F4/80$^+$ macrophages isolated from ovarian WAT from *Ext1*$^{F/F}$ or *Ext1*$^{\Delta Lyz2}$ mice fed a chow diet; n = 4 to 5/group with each being a pool of n = 2–4 mice.

(D) Experimental design for (E) and (F).

(E) Mitochondria capture by peritoneal macrophages 1 or 2 days after injection; n = 5/group.

(F) OCR of purified F4/80$^+$ peritoneal macrophages on day 1. N = 4/group.

(G) Experimental design for (H)–(J).

(H–J) (H) Basal, (I) maximal, and (J) ATP production-linked respiration (n = 6–10/group). For (E) and (H)–(J), two-way ANOVA with Sidak post hoc tests. For (A) and (F), two-way ANOVA with Sidak post hoc tests for each condition. For (B) and (C), Student's t tests. Mean ± SEM. *p < 0.05, **p < 0.01, ***p < 0.001, and ****p < 0.0001.

mitochondria transfer to WAT macrophages is not required for macrophage mitochondrial metabolism *in vivo*.

To test whether mitochondria transfer is sufficient to enhance aerobic respiration in macrophages *in vivo*, we purified mtD2 mitochondria and administered them by intraperitoneal injection to either WT or NDUFS4-deficient mice (Figure 5D). *Ndufs4*$^{-/-}$ mice have severely impaired Complex I activity and develop an inherited mitochondrial disease resembling Leigh Syndrome (Kruse et al., 2008). Using flow cytometry, we found that *Ndufs4*$^{+/+}$ and *Ndufs4*$^{-/-}$ peritoneal macrophages capture exogenous mtD2 mitochondria with similar frequencies (~90%) on day 1 post-treatment (Figure 5E). As early as day 2 post-treatment, the proportion of *Ndufs4*$^{+/+}$ cells that were mtD2+ was substantially lower than *Ndufs4*$^{-/-}$ cells, suggesting that metabolically compromised cells

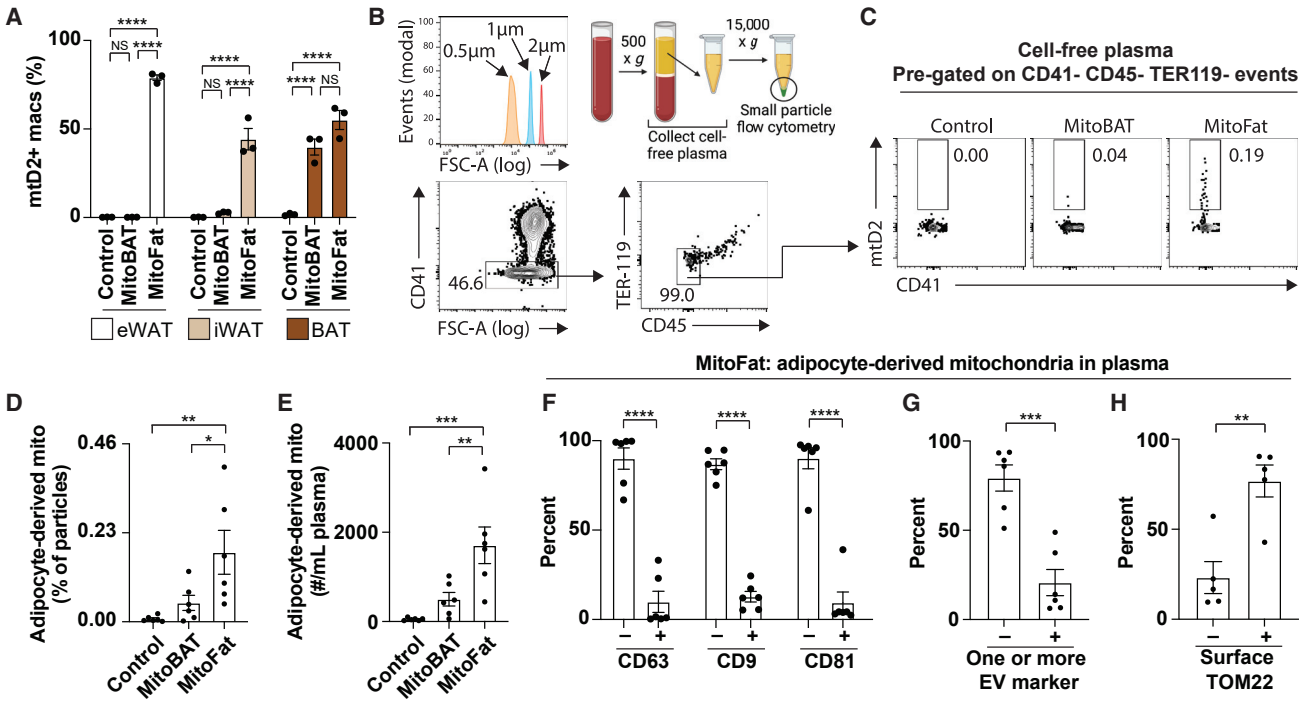

Figure 6. Adipocytes release micron-sized free mitochondria into blood

(A) Percentages of mtD2$^+$ macrophages in eWAT, iWAT, and BAT from *mtD2*$^{F/+}$ (control), MitoFat, and MitoBAT mice (n = 3/group).

(B) Small particle flow cytometry of plasma with size calibration beads and gating strategy.

(C–E) (C) Representative flow cytometry plots, (D) percentages, and (E) numbers of CD41− CD45− TER-119 mtD2+ adipocyte-derived mitochondria in plasma from control, MitoFat, and MitoBAT mice (n = 6/group).

(F–H) Percent of adipocyte-derived mitochondria in plasma that are positive or negative for (F) the extracellular vesicle (EV)-associated markers CD63, CD9, or CD81 (n = 6/group), (G) one or more of those (EV), or (H) the outer mitochondrial membrane protein TOM22 (n = 5/group).

For (A), (D), and (E), one-way ANOVA with Tukey post hoc test. For (F)–(H), Student's t tests. NS, not significant. Mean ± SEM. *p < 0.05, **p < 0.01, ***p < 0.001, and ****p < 0.0001.

may preserve exogenous mitochondria for a longer period. Next, we performed Seahorse assays on peritoneal F4/80$^+$ macrophages purified on day 1 post-treatment. Although there was little effect of exogenous mitochondria on aerobic respiration of *Ndufs4*$^{+/+}$ macrophages, exogenous mitochondria were able to completely restore aerobic respiration in *Ndufs4*$^{-/-}$ peritoneal macrophages (Figure 5F). These data indicate that exogenous purified mitochondria can restore aerobic respiration in cells that lack a critical mitochondrial enzyme *in vivo*.

To confirm this with another approach, we treated BV2 cells with rotenone plus antimycin A (R+A) or vehicle for 30 min, washed the cells, and then exposed them to purified mitochondria from WT or *Ndufs4*$^{-/-}$ mice for 1 h before performing Seahorse mitochondria stress test assays (Figure 5G). BV2 cells pre-treated with R+A for 30 min had reduced basal, maximal, and ATP production-linked mitochondrial respiration, and these phenotypes were completely restored by subsequent treatment with exogenous WT mitochondria for 1 h (Figures 5H–5J). Importantly, mitochondria from *Ndufs4*$^{-/-}$ mice failed to rescue R+A-treated BV2 cells. In vehicle-treated BV2 cells, neither WT nor *Ndufs4*$^{-/-}$ mitochondria had an appreciable effect on basal, maximal, or ATP-linked mitochondrial respiration. Collectively, these data suggest that healthy macrophages may take up exogenous mitochondria without prominently utilizing them for aerobic respiration, whereas metabolically stressed cells can capture and utilize exogenous mitochondria to support aerobic respiration.

LCFA-mediated inhibition of mitochondria uptake by macrophages promotes the release of adipocyte-derived mitochondria into the blood

To test whether we could directly measure adipocyte-derived mitochondria in blood and identify whether they were derived from white or brown adipocytes, we generated brown-adipocyte-specific mitochondria reporter (MitoBAT) mice, where the mtD2 reporter construct is driven by Uncoupling protein 1 (UCP1)-Cre, and compared them with MitoFat mice. First, we examined mitochondria transfer from adipocytes to macrophages in eWAT, iWAT, and BAT. We observed substantial adipocyte-to-macrophage mitochondria transfer in eWAT and iWAT of MitoFat mice, but not MitoBAT mice (Figure 6A), consistent with prior reports that the Ucp1-Cre is expressed in brown, but not white or beige, adipocytes in mice housed at room temperature (Kong et al., 2014). However, in BAT, we observed that approximately 50%–60% of macrophages were mtD2+ in both MitoFat and MitoBAT mice. These data indicate that MitoBAT mice have labeled mitochondria specifically in brown adipocytes.

Next, we performed small particle flow cytometry on cell-free plasma to examine circulating adipocyte-derived mitochondria

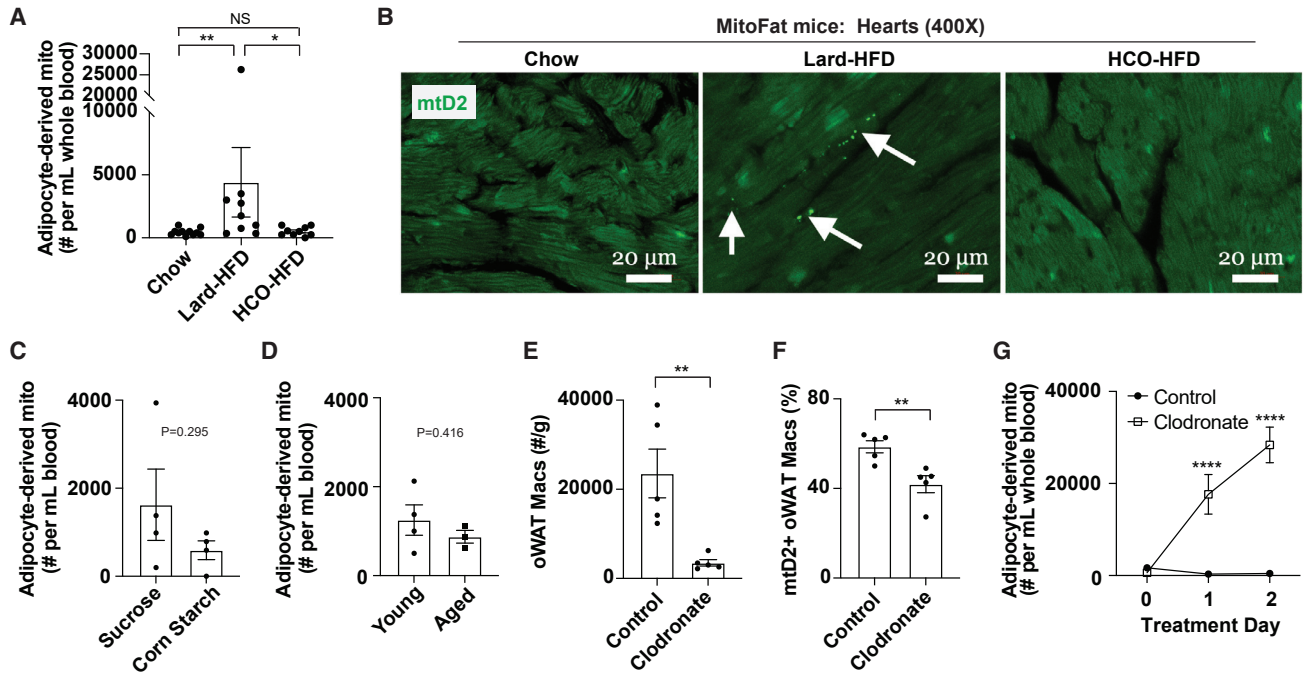

Figure 7. Macrophages limit the release of adipocyte-derived mitochondria into the blood

(A and B) Numbers of adipocyte-derived mitochondria in blood and (B) representative confocal microscopy of native mtD2 signal in hearts from MitoFat mice fed a chow (n = 11), lard-HFD (n = 9), or HCO-HFD (n = 9) for 9 to 10 weeks.

(C and D) Numbers of adipocyte-derived mitochondria in the blood of MitoFat mice (C) fed a high-sucrose or corn-starch diet for 12 weeks (n = 4/group) or (D) that were young (4 to 5 months old; n = 4) or aged (19 months old; n = 3) and were fed a normal chow diet.

(E–G) MitoFat mice were treated with control (n = 5) or clodronate-loaded liposomes (n = 5) twice daily for 2 days. (E) Numbers of macrophages per gram of WAT. (F) Percentage of remaining macrophages that are mtD2+. (G) Numbers of adipocyte-derived mitochondria in blood 0, 1, or 2 days after treatment.

For (A), one-way ANOVA with Tukey post hoc test. For (C)–(F), Student's t test. For (G), two-way ANOVA with repeated measures and Sidak post hoc testing comparing the two groups each day. Mean ± SEM. NS, not significant. *$p < 0.05$, **$p < 0.01$, and ****$p < 0.0001$.

(Figure 6B) from MitoFat or MitoBAT mice. We detected events ~1 μm in diameter (Figure 6B), with a limit of detection of ~0.4 μm on our flow cytometer. Therefore, this technique can detect microparticles and free mitochondria, but not smaller EVs from adipocytes such as those reported by Crewe et al. (2021) and Rosina et al. (2022). We gated on particles that lacked CD41, TER-119, and CD45 to exclude contaminating platelets, red blood cells, and immune cell fragments (Figure 6B). We observed mtD2+ particles, which we interpret to be adipocyte-derived mitochondria, in cell-free plasma from MitoFat mice that were more abundant in frequency (Figure 6D) and number (Figure 6E) than MitoBAT mice or controls. Most adipocyte-derived mitochondria in blood were negative for the EV markers CD63, CD9, or CD81 (Figure 6F). These markers were previously reported to be found on small EVs containing mitochondria from white and brown adipocytes (Crewe et al., 2021; Rosina et al., 2022). The majority of circulating adipocyte-derived mitochondria (~75% on average) were negative for all three of these EV markers (Figure 6G) and were positive for the outer mitochondrial membrane (OMM) protein TOM22 (Figure 6H). These data indicate that in lean mice, adipocytes release free mitochondria into the blood at low levels.

When MitoFat mice were fed a lard-HFD, a condition where mitochondria transfer from adipocytes to eWAT macrophages is impaired, there was a significant increase in adipocyte-derived mitochondria in blood (Figure 7A). This did not occur in HCO-HFD-fed MitoFat mice, a condition where mitochondria transfer is not impaired. Confocal microscopy of perfused hearts from MitoFat mice fed a lard-HFD, but not a normal chow diet or HCO-HFD contained mtD2+ puncta ~1 μm in size (Figure 7B), supporting that adipocyte-derived mitochondria released with lard-HFD feeding may be captured by cells in the heart, as has been reported (Crewe et al., 2021). Adipocyte-derived mitochondria in blood were not increased in corn-starch-diet-associated obesity (Figure 7C) or aging-associated obesity (Figure 7D), conditions without impaired mitochondria transfer to macrophages. These data suggest that suppression of mitochondria transfer to macrophages may lead to the release of adipocyte-derived mitochondria into circulation. To test this hypothesis, we depleted macrophages in WAT with clodronate-loaded or control liposomes (Figure 7E). Clodronate liposomes also inhibited mitochondria transfer from adipocytes to the small amount of remaining oWAT macrophages (Figure 7F). Strikingly, macrophage depletion was sufficient to markedly increase adipocyte-derived mitochondria in blood over 200-fold, whereas control liposomes had no effect (Figure 7G). These data indicate that inhibition of mitochondria transfer to macrophages with dietary LCFAs or clodronate liposome treatment leads to release of adipocyte-derived mitochondria into the blood.

DISCUSSION

Here, we find that adipocytes may transfer their mitochondria to a variety of cell types and that this process is influenced by tissue, cell type, and diet. Macrophages are the dominant recipients of adipocyte-derived mitochondria in white, beige, and brown fat. By comparing adipocyte-derived mitochondria transfer axes in aging-associated obesity and two different types of HFD-induced obesity, we found that dietary LCFAs can directly impair the ability of macrophages to take up mitochondria in an HS-dependent manner that is independent of CD36. Consequently, adipocyte-derived mitochondria are instead diverted into the blood in the setting of a lard-HFD (enriched in LCFAs) for delivery to distant organs, such as the heart. Other forms of obesity, including an HCO-HFD with low LCFA content, aging, and a corn-starch-enriched diet, do not affect mitochondria transfer from adipocytes to macrophages or promote the release of adipocyte-derived mitochondria into circulation. This indicates that dietary lipids may be a relatively specific class of signal that determines whether adipocyte-derived mitochondria are transferred locally to macrophages or systemically to distant organs.

These data are consistent with prior studies indicating that adipocyte-derived mitochondria can circulate in blood in small EVs and elicit an antioxidant response program in the heart to defend against cardiometabolic stress (Crewe et al., 2021). The mitochondria released from adipocytes were previously thought to be exclusively in small EVs. Using flow cytometry of larger 0.5–2 μm-sized particles in plasma, we also observed some adipocyte mitochondria in EVs. However, the majority of the large circulating mitochondria from adipocytes were negative for the EV markers CD63, CD9, and CD81 but positive for the OMM protein TOM22. These data suggest that most of the micron-sized adipocyte-derived mitochondria in the blood are free mitochondria. Furthermore, by comparing MitoBAT and MitoFat mice, we found that adipocyte mitochondria circulating in blood are mostly derived from white adipocytes. Together with the studies by Crewe et al. (2021), our data indicate that there are heterogeneous types of adipocyte-derived mitochondria in blood, with some in small or large EVs and some that are naked (i.e., free). Similar heterogeneity is known to occur in the context of platelets, which release both free and EV-associated mitochondria when activated (Boudreau et al., 2014).

The function of mitochondria transfer is likely context specific. For example, in the setting of ischemic stroke, astrocytes donate functional mitochondria to neurons to support their survival and limit stroke pathology (Hayakawa et al., 2016). Exogenous purified mitochondria are also able to rescue aerobic respiration in ρ^0 cells that lack fully functional mitochondria (Kim et al., 2018). However, we found that genetic disruption of HS-mediated mitochondria transfer to macrophages did not affect WAT macrophage mitochondrial metabolism. In addition, inducing capture of exogenous purified mitochondria appeared to have little effect on mitochondrial metabolism of both WT peritoneal macrophages *in vivo* and healthy BV2 cells *in vitro*. These observations suggest that mitochondria transfer is neither necessary nor sufficient for normal macrophage metabolic fitness under steady-state conditions. Interestingly, metabolically compromised macrophages that lack NDUFS4 or that were exposed to rotenone plus antimycin A had restored aerobic respiration with a single dose of exogenous purified mitochondria. Thus, metabolically injured macrophages may utilize mitochondria obtained from other cells to preserve cellular metabolism. It remains to be determined whether mitochondria transfer contributes to the metabolism or function of macrophages in obese adipose tissue.

Intercellular mitochondria transfer may also have functional consequences for donor cells. In BAT, brown adipocytes release oxidatively damaged mitochondrial components in small EVs for capture and degradation by macrophages (Rosina et al., 2022). Preventing mitochondria transfer to macrophages leads to failure of thermogenesis in BAT by inhibiting the expression of peroxisome proliferator-activated receptor (PPAR) target genes in brown adipocytes. Cardiomyocytes also release damaged mitochondria in large EVs (exophers) for degradation by macrophages to maintain normal cardiac function (Nicolás-Ávila et al., 2020). These studies suggest that parenchymal cells may license macrophages to perform mitophagy of exported mitochondria. Our data indicate that at steady state, a function of mitochondria transfer to macrophages in WAT may be to sequester and possibly eliminate mitochondria released by adipocytes, thereby limiting the release of adipocyte-derived mitochondria into the blood. LCFA inhibition of mitochondria uptake by WAT macrophages or depletion of WAT macrophages allows adipocyte mitochondria to be diverted into the bloodstream. In the case of lard-HFD feeding, our data and those by Crewe et al. (2021) indicate that adipocyte-derived mitochondria in blood are taken up by distant organs, such as the heart. This suggests that regulating the efficiency of mitochondria transfer to macrophages may determine the extent to which stromal and/or parenchymal cells release their mitochondria into the blood to support inter-organ cellular communication. Although it has been reported that adipocyte-derived mitochondria can promote metabolic adaptation in the heart by hormesis in an acute setting (Crewe et al., 2021), future studies are needed to study the functional impact of adipocyte-derived mitochondria on the heart and other organs in chronic diseases.

Our findings also indicate that ECs may be a major recipient of adipocyte-derived mitochondria, especially in BAT. Maintenance of the vascular bed is essential for preserving the thermogenic function of brown adipocytes, and both HFD-induced obesity and disruption of VEGF-A signaling leads to vascular rarefaction and whitening in BAT (Shimizu et al., 2014; Xue et al., 2009). Recent studies suggest that cell-free mitochondria may contribute to angiogenesis via multiple mechanisms. For example, administration of purified mesenchymal stem cell (MSC) mitochondria into infarcted hearts was associated with increased blood vessel density during the repair process, and these exogenous mitochondria were captured by heart ECs (Liang et al., 2022). Purified MSC mitochondria also promoted the proliferation of and alleviated oxidative stress in human umbilical vein ECs (Liang et al., 2022). In addition, it was shown that platelets can deliver mitochondria to MSCs in the setting of wound healing, driving production of pro-angiogenic factors such as VEGF-A that promote EC responses and revascularization of wounded skin (Levoux et al., 2021). It is not known whether adipocyte-to-EC mitochondria transfer regulates angiogenesis in white, beige, or brown fat or whether this transfer process

enables delivery of adipocyte-derived mitochondria into or from the circulation to distant organs and cells.

Recently, several efforts have been made to leverage the biology of intercellular mitochondria transfer to treat human diseases. For example, it has been shown that transfusing purified mitochondria leads to mitochondria capture by cardiomyocytes, improved cardiomyocyte bioenergetics, and reduced ischemia-reperfusion injury (IRI) in mammalian models of heart ischemia (Ali Pour et al., 2020; Masuzawa et al., 2013; McCully et al., 2009). Administering mitochondria to patients on extracorporeal membrane oxygenation (ECMO) therapy was tolerated (Emani et al., 2017) and was associated with faster weaning from ECMO support and less severe IRI (Guariento et al., 2021). In addition, it has been shown that exposing human cell products to purified mitochondria can metabolically reprogram their function. For example, hematopoietic stem cells (HSCs) exposed to purified mitochondria *ex vivo* are better able to engraft in recipients (Jacoby et al., 2021). In addition, human CD4 T cells exposed to healthy mitochondria produce less pro-inflammatory cytokines and drive less severe joint disease in a humanized mouse model of rheumatoid arthritis (Giwa and Brestoff, 2022; Wu et al., 2021). A potential implication of our studies is that the effectiveness of mitochondria transfer-associated therapies may depend on dietary metabolites such as lipids.

In summary, we found that in lean mice, adipocytes predominantly transfer their mitochondria to macrophages in adipose to limit the release of adipocyte-derived mitochondria into the blood. LCFAs in a lard-HFD inhibit mitochondria capture by adipose-resident macrophages, diverting adipocyte-derived mitochondria into the blood in EVs and as free mitochondria. Adipocyte-derived mitochondria in blood are distributed to distant organs, such as the heart, which is known to elicit a protective antioxidant response to defend against cardiometabolic stress (Crewe et al., 2021). These findings indicate that dietary lipids regulate mitochondria capture by macrophages to determine whether exported mitochondria from adipocytes are sequestered locally in the tissue or distributed to distant organs to support inter-organ metabolic adaptation to nutrient stress.

Limitations of the study

The multidimensional spectral flow cytometry panels used in these studies were designed to identify as many cell populations as possible but cannot spatially resolve the location of transferred mitochondria. It is possible that some of the putative mitochondria transfer axes reported here reflect mitochondria binding to the surface of the recipient cell type rather than internalization. In prior work (Brestoff et al., 2021), we used intravital 2-photon microscopy to visualize mitochondria transfer occurring from adipocytes to macrophages in gonadal WAT *in vivo*, and additional studies are needed to verify and characterize the biological functions of the putative mitochondria transfer axes reported here. Another limitation is that our data identify recipient cells at a given point in time and do not detect whether mitochondria transfer occurs via an intermediate cell type. We identified that one function of mitochondria transfer to macrophages is to limit the release of adipocyte-derived mitochondria into the blood. Although adipocyte-derived mitochondria can be identified in the heart (Crewe et al., 2021), the distribution of adipocyte-derived mitochondria to other organ systems is not yet known. Although our data suggest that dietary LCFA inhibition of mitochondria transfer to macrophages does not lead to redistribution of adipocyte-derived mitochondria to other cells in WAT stromal vascular fraction (SVF), it is possible that adipocytes could potentially recapture released mitochondria, as can occur with brown adipocytes (Rosina et al., 2022).

STAR★METHODS

Detailed methods are provided in the online version of this paper and include the following:

- KEY RESOURCES TABLE
- RESOURCE AVAILABILITY
  - Lead contact
  - Materials availability
  - Data and code availability
- EXPERIMENTAL MODEL AND SUBJECT DETAILS
  - Mouse models
  - Method details
  - Spectral flow cytometry
  - High-dimensional analyses of flow cytometry data
  - Detection of cell-free mitochondria in whole blood and plasma
  - Clodronate liposome depletion of macrophages
  - Histologic analyses of adipose and heart
  - Fatty acid (FA)-conjugation to bovine serum albumin (BSA)
  - BV2 cell culture
  - Generation of bone marrow-derived macrophages (BMDMs)
  - Isolation of purified mitochondria
  - Mitochondria uptake assay
  - Administration of purified mitochondria to mice and isolation of peritoneal macrophages
  - Seahorse mitochondrial stress test assays
  - Statistics

SUPPLEMENTAL INFORMATION

Supplemental information can be found online at https://doi.org/10.1016/j.cmet.2022.08.010.

ACKNOWLEDGMENTS

J.R.B. is supported by the National Institutes of Health (NIH) Common Fund via the NIH Director's Early Independence Award (DP5 OD028125), Burroughs Wellcome Fund Career Award for Medical Scientists (1019648), and National Institute for Allergy and Infectious Diseases (NIAID R01AI168044). Additional support was provided by NIH R00DK122019 (to C.C.), R01 HL045095 (to N.A.A.), T32 HL007081 (to B.Q.Y.), K08 HL159359 (to B.J.K.), and National Science Foundation (NSF) grant #DGE-1745038 / #DGE-2139839 (to M.M.C.). The anti-HS-biotin antibody was a generous gift from AMS Biotechnology Ltd (Abingdon, England). We thank Dr. Michael S. Diamond and Dr. Hongming Ma (both WashU) for providing sgGfp and sgExt1 edited BV2 cells and Drs. Brian S. Kim (Mt. Sinai School of Medicine) and Craig Wilen (Yale) for valuable discussion.

AUTHOR CONTRIBUTIONS

J.R.B. conceived of the project. N.B., W.J., R.G., R.L.F., J.R.M., E.C.W., B.J.K., M.M.C., B.Q.Y., J.M.S., A.L.B., C.C., and J.R.B. generated data and key resources and performed experiments. N.B. wrote the code and performed all bioinformatic analyses. N.B., W.J., R.G., and J.R.B. designed experiments, analyzed data, and wrote the paper. O.O., J.A.-B., S.C.M., T.P., and N.A.A. provided key resources. B.J.K., O.O., J.A.-B., M.N.A., A.L.B., S.C.M., N.A.A., J.S., K.L., and C.C. contributed to data analysis and interpretation and provided critical scientific advice. All authors contributed to data interpretation and read, edited, and approved the manuscript.

DECLARATION OF INTERESTS

J.R.B. has a pending patent application related to intercellular mitochondria transfer for the treatment of mitochondrial disorders, is a consultant for DeciBio and Flagship Pioneering, and is a scientific advisor to LUCA Science, Inc.

Received: August 24, 2021
Revised: June 6, 2022
Accepted: August 15, 2022
Published: September 6, 2022

REFERENCES

Al Amir Dache, Z., Otandault, A., Tanos, R., Pastor, B., Meddeb, R., Sanchez, C., Arena, G., Lasorsa, L., Bennett, A., Grange, T., et al. (2020). Blood contains circulating cell-free respiratory competent mitochondria. FASEB J. *34*, 3616–3630. https://doi.org/10.1096/fj.201901917RR.

Ali Pour, P., Kenney, M.C., and Kheradvar, A. (2020). Bioenergetics consequences of mitochondrial transplantation in cardiomyocytes. J. Am. Heart Assoc. *9*, e014501. https://doi.org/10.1161/JAHA.119.014501.

Alkhouri, N., Gornicka, A., Berk, M.P., Thapaliya, S., Dixon, L.J., Kashyap, S., Schauer, P.R., and Feldstein, A.E. (2010). Adipocyte apoptosis, a link between obesity, insulin resistance, and hepatic steatosis. J. Biol. Chem. *285*, 3428–3438. https://doi.org/10.1074/jbc.M109.074252.

Amend, S.R., Valkenburg, K.C., and Pienta, K.J. (2016). Murine hind limb long bone dissection and bone marrow isolation. Jove, e53936. https://doi.org/10.3791/53936.

Boudreau, L.H., Duchez, A.C., Cloutier, N., Soulet, D., Martin, N., Bollinger, J., Paré, A., Rousseau, M., Naika, G.S., Lévesque, T., et al. (2014). Platelets release mitochondria serving as substrate for bactericidal group IIA-secreted phospholipase A2 to promote inflammation. Blood *124*, 2173–2183. https://doi.org/10.1182/blood-2014-05-573543.

Brestoff, J.R. (2017). Isolation of immune cells from adipose tissue for flow cytometry. In Thermogenic fat: methods and protocols, J. Wu, ed. (Springer), pp. 49–59. https://doi.org/10.1007/978-1-4939-6820-6_6.

Brestoff, J.R., and Artis, D. (2015). Immune regulation of metabolic homeostasis in health and disease. Cell *161*, 146–160. https://doi.org/10.1016/j.cell.2015.02.022.

Brestoff, J.R., Kim, B.S., Saenz, S.A., Stine, R.R., Monticelli, L.A., Sonnenberg, G.F., Thome, J.J., Farber, D.L., Lutfy, K., Seale, P., and Artis, D. (2015). Group 2 innate lymphoid cells promote beiging of white adipose tissue and limit obesity. Nature *519*, 242–246. https://doi.org/10.1038/nature14115.

Brestoff, J.R., Wilen, C.B., Moley, J.R., Li, Y., Zou, W., Malvin, N.P., Rowen, M.N., Saunders, B.T., Ma, H., Mack, M.R., et al. (2021). Intercellular mitochondria transfer to macrophages regulates white adipose tissue homeostasis and is impaired in obesity. Cell Metab. *33*, 270–282.e8. https://doi.org/10.1016/j.cmet.2020.11.008.

Busse, M., Feta, A., Presto, J., Wilén, M., Grønning, M., Kjellén, L., and Kusche-Gullberg, M. (2007). Contribution of EXT1, EXT2, and EXTL3 to heparan sulfate chain elongation. J. Biol. Chem. *282*, 32802–32810. https://doi.org/10.1074/jbc.M703560200.

Chang, J.C., Chang, H.S., Wu, Y.C., Cheng, W.L., Lin, T.T., Chang, H.J., Kuo, S.J., Chen, S.T., and Liu, C.S. (2019). Mitochondrial transplantation regulates antitumour activity, chemoresistance and mitochondrial dynamics in breast cancer. J. Exp. Clin. Cancer Res. *38*, 30. https://doi.org/10.1186/s13046-019-1028-z.

Chevrier, S., Crowell, H.L., Zanotelli, V.R.T., Engler, S., Robinson, M.D., and Bodenmiller, B. (2018). Compensation of signal spillover in suspension and imaging mass cytometry. Cell Syst. *6*, 612–620.e5. https://doi.org/10.1016/j.cels.2018.02.010.

Coats, B.R., Schoenfelt, K.Q., Barbosa-Lorenzi, V.C., Peris, E., Cui, C., Hoffman, A., Zhou, G., Fernandez, S., Zhai, L., Hall, B.A., et al. (2017). Metabolically activated adipose tissue macrophages perform detrimental and beneficial functions during diet-induced obesity. Cell Rep. *20*, 3149–3161. https://doi.org/10.1016/j.celrep.2017.08.096.

Crewe, C., Funcke, J.B., Li, S., Joffin, N., Gliniak, C.M., Ghaben, A.L., An, Y.A., Sadek, H.A., Gordillo, R., Akgul, Y., et al. (2021). Extracellular vesicle-based interorgan transport of mitochondria from energetically stressed adipocytes. Cell Metab. *33*, 1853–1868.e11. https://doi.org/10.1016/j.cmet.2021.08.002.

Dalmas, E., Clément, K., and Guerre-Millo, M. (2011). Defining macrophage phenotype and function in adipose tissue. Trends Immunol. *32*, 307–314. https://doi.org/10.1016/j.it.2011.04.008.

Dong, L.F., Kovarova, J., Bajzikova, M., Bezawork-Geleta, A., Svec, D., Endaya, B., Sachaphibulkij, K., Coelho, A.R., Sebkova, N., Ruzickova, A., et al. (2017). Horizontal transfer of whole mitochondria restores tumorigenic potential in mitochondrial DNA-deficient cancer cells. eLife *6*, e22187. https://doi.org/10.7554/eLife.22187.

Emani, S.M., Piekarski, B.L., Harrild, D., del Nido, P.J., and McCully, J.D. (2017). Autologous mitochondrial transplantation for dysfunction after ischemia-reperfusion injury. J. Thorac. Cardiovasc. Surg. *154*, 286–289. https://doi.org/10.1016/j.jtcvs.2017.02.018.

Evans, C.S., and Holzbaur, E.L.F. (2020). Degradation of engulfed mitochondria is rate-limiting in optineurin-mediated mitophagy in neurons. eLife *9*, e50260. https://doi.org/10.7554/eLife.50260.

Giwa, R., and Brestoff, J.R. (2022). Mitochondria transfer to CD4(+) T cells may alleviate rheumatoid arthritis by suppressing pro-inflammatory cytokine production. Immunometabolism *4*, e220009. https://doi.org/10.20900/immunometab20220009.

Griessinger, E., Moschoi, R., Biondani, G., and Peyron, J.F. (2017). Mitochondrial transfer in the leukemia microenvironment. Trends Cancer *3*, 828–839. https://doi.org/10.1016/j.trecan.2017.10.003.

Guariento, A., Piekarski, B.L., Doulamis, I.P., Blitzer, D., Ferraro, A.M., Harrild, D.M., Zurakowski, D., del Nido, P.J., McCully, J.D., and Emani, S.M. (2021). Autologous mitochondrial transplantation for cardiogenic shock in pediatric patients following ischemia-reperfusion injury. J. Thorac. Cardiovasc. Surg. *162*, 992–1001. https://doi.org/10.1016/j.jtcvs.2020.10.151.

Haghverdi, L., Lun, A.T.L., Morgan, M.D., and Marioni, J.C. (2018). Batch effects in single-cell RNA-sequencing data are corrected by matching mutual nearest neighbors. Nat. Biotechnol. *36*, 421–427. https://doi.org/10.1038/nbt.4091.

Hahne, F., LeMeur, N., Brinkman, R.R., Ellis, B., Haaland, P., Sarkar, D., Spidlen, J., Strain, E., and Gentleman, R. (2009). flowCore: a bioconductor package for high throughput flow cytometry. BMC Bioinformatics *10*, 106. https://doi.org/10.1186/1471-2105-10-106.

Hales, C., Carroll, M., Fryar, C., and Ogden, C. (2020). Prevalence of Obesity and Severe Obesity among Adults: United States, 2017–2018 (National Center for Health Statistics).

Hayakawa, K., Esposito, E., Wang, X., Terasaki, Y., Liu, Y., Xing, C., Ji, X., and Lo, E.H. (2016). Transfer of mitochondria from astrocytes to neurons after stroke. Nature *535*, 551–555. https://doi.org/10.1038/nature18928.

Hotamisligil, G.S. (2017). Inflammation, metaflammation and immunometabolic disorders. Nature *542*, 177–185. https://doi.org/10.1038/nature21363.

Huber, A.H., Kampf, J.P., Kwan, T., Zhu, B., and Kleinfeld, A.M. (2006). Fatty acid-specific fluorescent probes and their use in resolving mixtures of unbound free fatty acids in equilibrium with albumin. Biochemistry *45*, 14263–14274. https://doi.org/10.1021/bi060703e.

Islam, M.N., Das, S.R., Emin, M.T., Wei, M., Sun, L., Westphalen, K., Rowlands, D.J., Quadri, S.K., Bhattacharya, S., and Bhattacharya, J. (2012). Mitochondrial transfer from bone-marrow-derived stromal cells to pulmonary alveoli protects against acute lung injury. Nat. Med. *18*, 759–765. https://doi.org/10.1038/nm.2736.

Jackson, M.V., Morrison, T.J., Doherty, D.F., McAuley, D.F., Matthay, M.A., Kissenpfennig, A., O'Kane, C.M., and Krasnodembskaya, A.D. (2016). Mitochondrial transfer via tunneling nanotubes is an important mechanism by which mesenchymal stem cells enhance macrophage phagocytosis in the in vitro and in vivo models of ARDS. Stem Cells *34*, 2210–2223. https://doi.org/10.1002/stem.2372.

Jacoby, E., Ben Yakir-Blumkin, M., Blumenfeld-Kan, S., Brody, Y., Meir, A., Melamed-Book, N., Napso, T., Pozner, G., Saadi, E., Shabtay-Orbach, A., et al. (2021). Mitochondrial augmentation of CD34+ cells from healthy donors and patients with mitochondrial DNA disorders confers functional benefit. npj Regen. Med. *6*, 58. https://doi.org/10.1038/s41536-021-00167-7.

Kim, M.J., Hwang, J.W., Yun, C.K., Lee, Y., and Choi, Y.S. (2018). Delivery of exogenous mitochondria via centrifugation enhances cellular metabolic function. Sci. Rep. *8*, 3330. https://doi.org/10.1038/s41598-018-21539-y.

Kong, X., Banks, A., Liu, T., Kazak, L., Rao, R.R., Cohen, P., Wang, X., Yu, S., Lo, J.C., Tseng, Y.H., et al. (2014). IRF4 is a key thermogenic transcriptional partner of PGC-1α. Cell *158*, 69–83. https://doi.org/10.1016/j.cell.2014.04.049.

Kratz, M., Coats, B.R., Hisert, K.B., Hagman, D., Mutskov, V., Peris, E., Schoenfelt, K.Q., Kuzma, J.N., Larson, I., Billing, P.S., et al. (2014). Metabolic dysfunction drives a mechanistically distinct proinflammatory phenotype in adipose tissue macrophages. Cell Metab. *20*, 614–625. https://doi.org/10.1016/j.cmet.2014.08.010.

Kruse, S.E., Watt, W.C., Marcinek, D.J., Kapur, R.P., Schenkman, K.A., and Palmiter, R.D. (2008). Mice with mitochondrial complex I deficiency develop a fatal encephalomyopathy. Cell Metab. *7*, 312–320. https://doi.org/10.1016/j.cmet.2008.02.004.

Levoux, J., Prola, A., Lafuste, P., Gervais, M., Chevallier, N., Koumaiha, Z., Kefi, K., Braud, L., Schmitt, A., Yacia, A., et al. (2021). Platelets facilitate the wound-healing capability of mesenchymal stem cells by mitochondrial transfer and metabolic reprogramming. Cell Metab. *33*, 283–299.e9. https://doi.org/10.1016/j.cmet.2020.12.006.

Liang, X., Zhang, Y., Lin, F., Li, M., Li, X., Chen, Y., Liu, J., Meng, Q., Ma, X., Wang, E., et al. (2022). Direct administration of mesenchymal stem cell-derived mitochondria improves cardiac function after infarction via ameliorating endothelial senescence. Bioengineering Transla. Med. e10365. https://doi.org/10.1002/btm2.10365.

Lu, J., Zheng, X., Li, F., Yu, Y., Chen, Z., Liu, Z., Wang, Z., Xu, H., and Yang, W. (2017). Tunneling nanotubes promote intercellular mitochondria transfer followed by increased invasiveness in bladder cancer cells. Oncotarget *8*, 15539–15552. https://doi.org/10.18632/oncotarget.14695.

Lumeng, C.N., DelProposto, J.B., Westcott, D.J., and Saltiel, A.R. (2008). Phenotypic switching of adipose tissue macrophages with obesity is generated by spatiotemporal differences in macrophage subtypes. Diabetes *57*, 3239–3246. https://doi.org/10.2337/db08-0872.

Lumeng, C.N., Deyoung, S.M., Bodzin, J.L., and Saltiel, A.R. (2007). Increased inflammatory properties of adipose tissue macrophages recruited during diet-induced obesity. Diabetes *56*, 16–23. https://doi.org/10.2337/db06-1076.

Makki, K., Froguel, P., and Wolowczuk, I. (2013). Adipose tissue in obesity-related inflammation and insulin resistance: cells, cytokines, and chemokines. ISRN Inflamm. *2013*, 139239. https://doi.org/10.1155/2013/139239.

Marcelin, G., Ferreira, A., Liu, Y., Atlan, M., Aron-Wisnewsky, J., Pelloux, V., Botbol, Y., Ambrosini, M., Fradet, M., Rouault, C., et al. (2017). A PDGFRα-mediated switch toward CD9(high) adipocyte progenitors controls obesity-induced adipose tissue fibrosis. Cell Metab. *25*, 673–685. https://doi.org/10.1016/j.cmet.2017.01.010.

Martin, C., Chevrot, M., Poirier, H., Passilly-Degrace, P., Niot, I., and Besnard, P. (2011). CD36 as a lipid sensor. Physiol. Behav. *105*, 36–42. https://doi.org/10.1016/j.physbeh.2011.02.029.

Masuzawa, A., Black, K.M., Pacak, C.A., Ericsson, M., Barnett, R.J., Drumm, C., Seth, P., Bloch, D.B., Levitsky, S., Cowan, D.B., and McCully, J.D. (2013). Transplantation of autologously derived mitochondria protects the heart from ischemia-reperfusion injury. Am. J. Physiol. Heart Circ. Physiol. *304*, H966–H982. https://doi.org/10.1152/ajpheart.00883.2012.

McCully, J.D., Cowan, D.B., Pacak, C.A., Toumpoulis, I.K., Dayalan, H., and Levitsky, S. (2009). Injection of isolated mitochondria during early reperfusion for cardioprotection. Am. J. Physiol. Heart Circ. Physiol. *296*, H94–H105. https://doi.org/10.1152/ajpheart.00567.2008.

McNelis, J.C., and Olefsky, J.M. (2014). Macrophages, immunity, and metabolic disease. Immunity *41*, 36–48. https://doi.org/10.1016/j.immuni.2014.05.010.

Mistry, J.J., Marlein, C.R., Moore, J.A., Hellmich, C., Wojtowicz, E.E., Smith, J.G.W., Macaulay, I., Sun, Y., Morfakis, A., Patterson, A., et al. (2019). ROS-mediated PI3K activation drives mitochondrial transfer from stromal cells to hematopoietic stem cells in response to infection. Proc. Natl. Acad. Sci. USA *116*, 24610–24619. https://doi.org/10.1073/pnas.1913278116.

Nicolás-Ávila, J.A., Lechuga-Vieco, A.V., Esteban-Martínez, L., Sánchez-Díaz, M., Díaz-García, E., Santiago, D.J., Rubio-Ponce, A., Li, J.L., Balachander, A., Quintana, J.A., et al. (2020). A network of macrophages supports mitochondrial homeostasis in the heart. Cell *183*, 94–109.e23. https://doi.org/10.1016/j.cell.2020.08.031.

Nowicka, M., Krieg, C., Crowell, H., Weber, L., Hartmann, F., Guglietta, S., Becher, B., Levesque, M., and Robinson, M. (2019). CyTOF workflow: differential discovery in high-throughput high-dimensional cytometry datasets [version 3; peer review: 2 approved]. F1000 Res. *6*, 748. https://doi.org/10.12688/f1000research.11622.3.

Olefsky, J.M., and Glass, C.K. (2010). Macrophages, inflammation, and insulin resistance. Annu. Rev. Physiol. *72*, 219–246. https://doi.org/10.1146/annurev-physiol-021909-135846.

Orchard, R.C., Wilen, C.B., Doench, J.G., Baldridge, M.T., McCune, B.T., Lee, Y.-C.J., Lee, S., Pruett-Miller, S.M., Nelson, C.A., Fremont, D.H., and Virgin, H.W. (2016). Discovery of a proteinaceous cellular receptor for a norovirus. Science *353*, 933–936. https://doi.org/10.1126/science.aaf1220.

Pepino, M.Y., Kuda, O., Samovski, D., and Abumrad, N.A. (2014). Structure-function of CD36 and importance of fatty acid signal transduction in fat metabolism. Annu. Rev. Nutr. *34*, 281–303. https://doi.org/10.1146/annurev-nutr-071812-161220.

Pham, A.H., McCaffery, J.M., and Chan, D.C. (2012). Mouse lines with photo-activatable mitochondria to study mitochondrial dynamics. Genesis *50*, 833–843. https://doi.org/10.1002/dvg.22050.

Rebbeck, C.A., Leroi, A.M., and Burt, A. (2011). Mitochondrial capture by a transmissible cancer. Science *331*, 303. https://doi.org/10.1126/science.1197696.

Rosina, M., Ceci, V., Turchi, R., Chuan, L., Borcherding, N., Sciarretta, F., Sánchez-Díaz, M., Tortolici, F., Karlinsey, K., Chiurchiù, V., et al. (2022). Ejection of damaged mitochondria and their removal by macrophages ensure efficient thermogenesis in brown adipose tissue. Cell Metab. *34*, 533–548.e12. https://doi.org/10.1016/j.cmet.2022.02.016.

Saltiel, A.R., and Olefsky, J.M. (2017). Inflammatory mechanisms linking obesity and metabolic disease. J. Clin. Invest. *127*, 1–4. https://doi.org/10.1172/JCI92035.

Schuyler, R.P., Jackson, C., Garcia-Perez, J.E., Baxter, R.M., Ogolla, S., Rochford, R., Ghosh, D., Rudra, P., and Hsieh, E.W.Y. (2019). Minimizing batch effects in mass cytometry data. Front. Immunol. *10*, 2367. https://doi.org/10.3389/fimmu.2019.02367.

Scozzi, D., Ibrahim, M., Liao, F., Lin, X., Hsiao, H.M., Hachem, R., Tague, L.K., Ricci, A., Kulkarni, H.S., Huang, H.J., et al. (2019). Mitochondrial damage-associated molecular patterns released by lung transplants are associated with primary graft dysfunction. Am. J. Transplant. *19*, 1464–1477. https://doi.org/10.1111/ajt.15232.

Shimizu, I., Aprahamian, T., Kikuchi, R., Shimizu, A., Papanicolaou, K.N., MacLauchlan, S., Maruyama, S., and Walsh, K. (2014). Vascular rarefaction mediates whitening of brown fat in obesity. J. Clin. Invest. *124*, 2099–2112. https://doi.org/10.1172/JCI71643.

Spector, A.A., Fletcher, J.E., and Ashbrook, J.D. (1971). Analysis of long-chain free fatty acid binding to bovine serum albumin by determination of stepwise equilibrium constants. Biochemistry *10*, 3229–3232. https://doi.org/10.1021/bi00793a011.

Spees, J.L., Olson, S.D., Whitney, M.J., and Prockop, D.J. (2006). Mitochondrial transfer between cells can rescue aerobic respiration. Proc. Natl. Acad. Sci. USA *103*, 1283–1288. https://doi.org/10.1073/pnas.0510511103.

Stott, N.L., and Marino, J.S. (2020). High fat rodent models of type 2 diabetes: from rodent to human. Nutrients *12*, 3650. https://doi.org/10.3390/nu12123650.

Sun, K., Kusminski, C.M., and Scherer, P.E. (2011). Adipose tissue remodeling and obesity. J. Clin. Invest. *121*, 2094–2101. https://doi.org/10.1172/JCI45887.

Wang, M.-E., Singh, B.K., Hsu, M.-C., Huang, C., Yen, P.M., Wu, L.-S., Jong, D.-S., and Chiu, C.-H. (2017). Increasing dietary medium-chain fatty acid ratio mitigates high-fat diet-induced non-alcoholic steatohepatitis by regulating autophagy. Sci. Rep. *7*, 13999. https://doi.org/10.1038/s41598-017-14376-y.

Wellen, K.E., and Hotamisligil, G.S. (2003). Obesity-induced inflammatory changes in adipose tissue. J. Clin. Invest. *112*, 1785–1788. https://doi.org/10.1172/JCI20514.

Wu, B., Zhao, T.V., Jin, K., Hu, Z., Abdel, M.P., Warrington, K.J., Goronzy, J.J., and Weyand, C.M. (2021). Mitochondrial aspartate regulates TNF biogenesis and autoimmune tissue inflammation. Nat. Immunol. *22*, 1551–1562. https://doi.org/10.1038/s41590-021-01065-2.

Xue, Y., Petrovic, N., Cao, R., Larsson, O., Lim, S., Chen, S., Feldmann, H.M., Liang, Z., Zhu, Z., Nedergaard, J., et al. (2009). Hypoxia-independent angiogenesis in adipose tissues during cold acclimation. Cell Metab. *9*, 99–109. https://doi.org/10.1016/j.cmet.2008.11.009.

Yamato, M., Shiba, T., Yoshida, M., Ide, T., Seri, N., Kudou, W., Kinugawa, S., and Tsutsui, H. (2007). Fatty acids increase the circulating levels of oxidative stress factors in mice with diet-induced obesity via redox changes of albumin. FEBS J. *274*, 3855–3863. https://doi.org/10.1111/j.1742-4658.2007.05914.x.

Zhu, T.-T., Zhang, Y., Luo, X.-A., Wang, S.-Z., Jia, M.-Q., and Chen, Z.-X. (2018). Difference in binding of long- and medium-chain fatty acids with serum albumin: the role of macromolecular crowding effect. J. Agric. Food Chem. *66*, 1242–1250. https://doi.org/10.1021/acs.jafc.7b03548.

STAR★METHODS

KEY RESOURCES TABLE

REAGENT or RESOURCE	SOURCE	IDENTIFIER
Antibodies		
SiglecF BV421	BD Biosciences	Cat# 562681
CD44 Super Bright 436	eBioscience	Cat# 62-044-180
CD11b Pacific Blue	BioLegend	Cat# 101224
IL-33Rα-biotin	BioLegend	Cat# 145308
Streptavidin (2°) BV480	BD Horizon	Cat# 564876
MHC-II (I-A/I-E) BV510	BioLegend	Cat# 107636
Ly6C BV570	BioLegend	Cat# 128030
KLRG1 BV605	BioLegend	Cat# 138419
F4/80 BV650	BioLegend	Cat# 123149
Ly6G BV711	BioLegend	Cat# 127643
CD3 BV750	BioLegend	Cat# 100249
CD206 BV785	BioLegend	Cat# 141729
TCRβ AF488	BioLegend	Cat# 109215
CD8 Spark Blue 550	BioLegend	Cat# 100780
CD45 PerCP	BioLegend	Cat# 103130
CD71 PerCP-Cy5.5	BioLegend	Cat# 113816
NKp46 PerCP-eFluor 710	eBioscience	Cat# 46-3351-82
TCRγδ PE	BioLegend	Cat# 118108
CD64 PE/Dazzle 594	BioLegend	Cat# 139320
CD4 PE/Fire 640	BioLegend	Cat# 100482
CD62L PE-Cy5	BioLegend	Cat# 104410
CD11c PE-Cy5.5	eBioscience	Cat# 35-0114-82
CD25 PE-Cy7	BioLegend	Cat# 102016
CD9 APC	BioLegend	Cat# 124812
CD127 AF647	BioLegend	Cat# 135020
CD19 Spark NIR 685	BioLegend	Cat# 115568
CD90.2 AF700	BioLegend	Cat# 105320
CD5 BUV737	BD Horizon	Cat# 612809
NK1.1 APC/Fire 750	BioLegend	Cat# 108752
B220 APC/Fire 810	BioLegend	Cat# 103278
Heparan sulfate-biotin (high)	AMSbio	Cat# 370255-B-50-H
NK1.1 BV510	BioLegend	Cat# 108737
EpCAM BV605	BioLegend	Cat# 118227
B220 BV750	BioLegend	Cat# 103261
CD31 PerCP-Cy5.5	BioLegend	Cat# 102522 and Cat# 102420
CD95 PerCP-eFluor710	eBioscience	Cat# 46-0951-82
CD36 PE	BioLegend	Cat# 102605
CD140a (PDGFRA) PE-Cy5	BioLegend	Cat# 100482
LYVE-1 PE/Cy7	eBioscience	Cat# 25-0443-82
MHC-II PE/Fire 810	BioLegend	Cat# 107667
CD209b APC	eBioscience	Cat# 17-2093-82
CD34 AF-647	BioLegend	Cat# 119314
CD73 APC/Fire 750	BioLegend	Cat# 127221
CD38 APC/Fire 810	BioLegend	Cat# 102745

(*Continued on next page*)

Continued

REAGENT or RESOURCE	SOURCE	IDENTIFIER
CD41 BV421	BioLegend	Cat# 133911
TER-119 PB	BioLegend	Cat# 116231
CD45 PerCP/Cy5.5	BioLegend	Cat# 103131
CD81 PE	BioLegend	Cat# 104905
CD63 PE/Cy7	BioLegend	Cat# 143909
Goat anti-CD31	R&D Systems	Cat# AF3628
Anti-goat IgG AF594	Jackson ImmunoResearch	Cat# 705-585-147
Cleaved Caspase-3	Cell Signaling Technology	RRID:AB_2070042
Chemicals, peptides, and recombinant proteins		
Lard 60% high fat diet, irradiated	Research Diets, Inc.	Cat#D12492i
HCO 60% high fat diet, irradiated	Research Diets, Inc.	Cat#D00071501i
ACK Red Blood Cell Lysis Buffer	Gibco	Cat#A10492-01
High sucrose diet	Research Diets, Inc.	D12450B
Corn starch diet	Research Diets, Inc.	D12450K
PicoLab Rodent Diet 20	Lab Diet	53WU
Bovine Serum Albumin	Pierce	Cat#23209
Brilliant Stain Buffer	BD Horizon	Cat#566349
Collagenase type II	Sigma-Aldrich	Cat#C6885
Coomassie Plus Reagent	Pierce	Cat#23236
Delbuco's Modified Eagle Media (DMEM) with 4.5 g/L D-glucose, L-glutamine, and no sodium pyrophosphate	Gibco	Cat#11965-084
DPBS	Gibco	Cat#14190-136
EDTA, 0.5M, pH 8.0	Invitrogen	Cat#AM9260G
Fetal bovine serum (FBS)	Corning	Cat#35-010-CV
L-glutamine	Corning	Cat#25-005-CI
Penicillin-Streptomycin	Corning	Cat#30-002-CI
Trypan blue	Sigma-Aldrich	Cat#T8154
Trypsin-EDTA	Gibco	Cat#15400-054
Ultracomp eBeads Compensation Beads	Invitrogen	Cat#01-2222-42
SpectroFlow QC Beads, Lot 2003	Cytek	Cat#N7-97355-0A
ZombieNIR Fixable Viability Dye	BioLegend	Cat#423106
Fatty acid-free BSA, fraction V	Roche	Cat#10775835001
Dodecanoic acid (Lauric acid)	Sigma-Aldrich	Cat#L4250-100G
Myristic acid, Sigma Grade	Sigma-Aldrich	Cat#M3128-100G
Palmitic acid, ≥99%	Sigma-Aldrich	Cat#P0500-25G
Stearic acid, Grade I	Sigma-Aldrich	Cat#S4751-25G
Oleic acid, ≥99% (GC)	Sigma-Aldrich	Cat#O1008-1G
Linoleic acid, ≥99%	Sigma-Aldrich	Cat#L1376-1G
CMG14-12 media (1.3 μg/mL M-CSF)	Drs. Wei Zou and Steven L. Teitelbaum	n/a
Heparin (Grade I-A)	Sigma-Aldrich	Cat#H3149-1MU
Flow Cytometry Sub-Micron Size Reference Kit beads	Invitrogen	Cat#F13839
Control Liposomes for Clophosome, Neutral	FormuMax Scientific	Cat# F70101-N
Clophosome Clodronate Liposomes, Neutral	FormuMax Scientific	Cat# F70101C-N
4% PFA in PBS	Santa Cruz Biotechnology	Cat# sc-281692
Citrate buffer	Sigma-Aldrich	Cat# C9999
ImmPRESS HRP Universal PLUS Polymer Kit	Vector Laboratories	Cat# MP-7800
Hematoxylin	Vector Laboratories	Cat# H-3401
BLOXALL Endogenous Enzyme Blocking Solution	Vector Laboratories	Cat# SP-6000
Fluoromoutn-G with DAPI	Invitrogen	Cat# 00-4959-52

(*Continued on next page*)

Continued

REAGENT or RESOURCE	SOURCE	IDENTIFIER
OCT Compound	Fisher Healthcare	Cat# 4585
DAPI mounting, anti-fade solution	Vectashield	Cat# H-1200
DMEM without glucose	Corning	Cat# 17-207-CV
Glucose	Sigma	Cat# G8270-1KG
Sucrose	Sigma	Cat# S7903
anti-F4/80 MicroBeads UltraPure	Miltenyibiotec	Cat# 130-110-443
LS Columns	Miltenyibiotec	Cat# 130-042-401
QuadroMACS separator	Miltenyibiotec	Cat# 130-090-976
Seahorse XF HS PDL Miniplates	Agilent	Cat# 103727-100
Seahorse XFe96 PDL Microplates	Agilent	Cat# 103730-100
Poly-D-Lysine solution	Gibco	Cat# A38904-01
Seahorse XF DMEM Assay Media Pack	Agilent	Cat# 103680-100
Critical commercial assays		
Mitochondria Isolation Kit, Mouse Tissue	Miltenyi Biotec	Cat# 130-096-946
Seahorse XFp Cell Mito Stress Test Kit for use with Seahorse XF HS Mini and XFp analyzers	Agilent	Cat# 103010-100
Seahorse XF Cell Mito Stress Test Kit for use with Seahorse XFe/XF96 analyzers	Agilent	Cat# 103015-100
Deposited data		
Spectral flow cytometry data, unmixed (Figures 1B, 1D–1F, 2E, 3E, S1, S2D, S2E, S3G, and S3H)	This paper	https://doi.org/10.5281/zenodo.6929098
Source data for Figures 1C, 2A–2D, 3A–3D, 4, 5, 6, 7, S3E, and S3F	This paper	Data S1
Experimental models: Cell lines		
BV2 cells	Orchard et al. (2016)	n/a
Experimental models: Organisms/strains		
Adipoq$^{Cre/+}$	Jackson Labs	Stock no. 28020
MitoFat (*mtD2*$^{Flox/+}$;*Adipoq*$^{Cre/+}$)	Generated in house	n/a
MitoBAT (*mtD2*$^{Flox/+}$;*Ucp1*$^{Cre/+}$)	Generated in house	n/a
mtDendra2$^{Flox/+}$ (i.e., PhAM Flox, mtD2$^{Flox/+}$)	Jackson Labs	Stock no. 18385
Cd36$^{+/-}$	Jackson Labs	Stock no. 19006
Ucp1-Cre	Jackson Labs	Stock no. 024670
Ndufs4$^{+/-}$	Jackson Labs	Stock no. 027058
Oligonucleotides		
n/a		
Software and algorithms		
Prism 9	GraphPad Software, Inc.	n/a
BatchAdjust()	Schuyler et al. (2019)	n/a
flowCore (v2.1.4) R package	Hahne et al. (2009)	n/a
CATALYST (v1.14.0) R package	Chevrier et al. (2018); Nowicka et al. (2019)	n/a
bluster (v1.0.0) R package	Bioconductor	n/a
SpectroFlo (v1.0)	Cytek	n/a
fastMNN() function from the batchelor (v1.8.1) R package	Haghverdi et al. (2018)	n/a
All analytic code, including Clock Face Diagram code	This paper	https://doi.org/10.5281/zenodo.6929098

RESOURCE AVAILABILITY

Lead contact

Further information and requests for resources and reagents should be directed to and will be fulfilled by the lead contact, Jonathan R. Brestoff (brestoff@wustl.edu).

Materials availability

This study did not generate new unique reagents.

Data and code availability

- All data reported in this paper will be shared by the lead contact upon request. Source data for graphs are included in Data S1. Spectral flow cytometry data have been deposited at https://doi.org/10.5281/zenodo.6929098 and are publicly available as of the date of publication. DOIs are listed in the key resources table.
- All original code has been deposited at https://doi.org/10.5281/zenodo.6929098 and is publicly available as of the date of publication. DOIs are listed in the key resources table.
- Any additional information required to reanalyze the data reported in this paper is available from the lead contact upon request.

EXPERIMENTAL MODEL AND SUBJECT DETAILS

Mouse models

Adipocyte-specific mitochondria reporter (MitoFat) mice were generated as previously described (Brestoff et al., 2021). Briefly, *mtDendra2*$^{Flox/Flox}$ (PhAM Flox; referred to as *mtD2*$^{F/F}$; Jackson Laboratories, stock number 18385) were crossed to *Adipoq*$^{Cre/+}$ mice (Jackson Laboratories, stock number 28020) to generate MitoFat mice (*mtD2*$^{F/+}$*AdipoqCre*$^{+/-}$) or Cre-negative controls (*mtD2*$^{F/+}$). MitoBAT mice were generated by crossing *Ucp1*$^{Cre/+}$ (Jackson Laboratories, stock number 024670) to *mtD2*$^{F/F}$ mice. *mtD2*$^{F/F}$ mice express mtD2 under control of a ROSA26 Flox-STOP-Flox system, enabling expression of mtD2 in cells that express Cre recombinase (Pham et al., 2012). Female CD36-deficient mice were obtained from Jackson Laboratories (stock number 19006). *Ndufs4*$^{+/-}$ mice were obtained from Jackson Laboratories (stock number 027058) and were bred as heterozygotes x heterozygotes to obtain *Ndufs4*$^{+/+}$ and *Ndufs4*$^{-/-}$ mice. Mice were genotyped at Transnetyx using established primers and protocols. MitoFat and MitoBAT mice were male or female and were aged 4-5 months (young) or 19-24 months (aged) at the time of tissue harvest, as indicated. *Ndufs4*$^{+/+}$ or *Ndufs4*$^{-/-}$ mice were used at the ages of 5-6-weeks-old. MitoFat mice were fed a standard chow diet (LabDiet, PicoLab Rodent Diet 20, 53WU), 10% kcal fat chow with carbohydrates mostly from sucrose (Research Diets, catalog number D12450B), 10% kcal fat diet with carbohydrate mainly from corn starch (Research Diets, catalog number D12450K), 60% kcal fat HFD made from lard (Research Diets, Inc., catalog number D12492), or 60% kcal fat HFD made from hydrogenated coconut oil (Research Diets, catalog number D00071501), as indicated. All mice had *ad libitum access* to food and water and were maintained in a specific-pathogen-free facility with a 12h:12h light:dark cycle. Animals were randomly assigned to n=2-5 mice/group per experiment, except when indicated otherwise, and data represent at least 2 independent experiments that were pooled for analysis. Mice were euthanized using isoflurane immediately prior to harvesting inguinal white adipose tissue (iWAT), epididymal (e)WAT (males), ovarian (o)WAT (females), and interscapular brown adipose tissue (BAT). All experiments were carried out under the guidelines of the Institutional Animal Care and Use Committee (IACUC) at Washington University in St. Louis and were performed under IACUC-approved protocols.

Method details

Isolation of immune cells from mouse tissues

eWAT, iWAT, and BAT were finely minced and digested in 4 mL of 0.1% collagenase type II (Sigma-Aldrich, C6885) in high glucose DMEM contained in a 5 mL conical tube, as previously described (Brestoff, 2017; Brestoff et al., 2015). Digestion was performed at 37 °C for 60 min in an orbital shaker with rotation at 140 rpm while tilted at a 90°angle. Single-cell suspensions of eWAT, iWAT, or BAT were passed through a 100 mm nylon mesh filter, which was washed twice with 5 mL of Wash Media (DMEM with 5% FBS, 2 mM L-glutamine, and 100 U/mL Penicillin-Streptomycin). Cells were pelleted by centrifugation at 500 x *g* for 5 min at 4 °C. The floating adipocytes were aspirated, and the stromal vascular fraction (SVF) pellet was resuspended in 1 mL ACK Red Blood Cell (RBC) Lysis Buffer (Gibco) and incubated at room temperature for 3-5 min. RBC lysis was quenched with 10 mL Wash Media. SVF cells were pelleted as above and resuspended in wash media for subsequent staining for flow cytometric analyses.

Spectral flow cytometry

Cells were washed in 200 μL PBS and then stained in 50 μL of Zombie Near Infrared (NIR; 1:1,000; BioLegend) in PBS and incubated on ice for 5 min covered in foil. The reaction was quenched with 200 μL of FACS Buffer (PBS supplemented with 2.5% heat-inactivated FBS and 2.5 mM EDTA), and cells were pelleted as above. Cells were resuspended in 30 μL of 5 μg/mL FcBlock (rat anti-mouse CD16/32, clone 2.4G2, BD Biosciences) for 5 min before addition of 30 μL 2X stain cocktail (final concentration 1X, see below for antibody information and final dilutions) comprised of various fluorophore-conjugated antibodies in Brilliant Stain Buffer

(BD Biosciences) containing 5 μg/mL FcBlock. Cells were stained for 30 min on ice while protected from light and then washed 2 times in 200 μL FACS Buffer. The cells were resuspended in 60 μL Steptavidin-BV480 (BioLegend) in FACS Buffer and incubated on ice for 20 min while protected from light. Cells were washed 2 times in 200 μL FACS Buffer. Finally, the cells were resuspended in 200 μL FACS Buffer and were acquired live on a Cytek Aurora spectral flow cytometer equipped with 4 lasers (violet, blue, yellow/green, and red lasers). Two different panels were used for bioinformatic analyses: Panel 1 (Table S2) and Panel 2 (Table S3).

For comparison of mitochondria transfer from adipocytes to macrophages in weight-matched Lard-HFD vs HCO-HFD mice, two separate cohorts were used. They were stained with Panels 1 or 2, therefore it was not possible to generate directly comparable clockface diagrams that can be reliably pooled. Therefore, for weight-matched comparisons, we gated on live $CD45^+$ $SiglecF^-$ $F4/80^+$ $CD64^+$ macrophages in eWAT, iWAT, and BAT to determine the percentages of macrophages that were $mtD2^+$ for direct comparison.

High-dimensional analyses of flow cytometry data

Flow cytometry standard files normalized for batch effect using previously described *BatchAdjust()* (Schuyler et al., 2019) and a quantile-based approach. The resulting corrected data were loaded as a flowSet using the flowCore (v2.1.4) R package (Hahne et al., 2009). Fluorescent values were biexponentially transformed using the *estimateLogicle()*and *transform()* functions. The resulting FlowSet was then converted into a SingleCellExperiment object using the CATALYST (v1.14.0) R package (Chevrier et al., 2018; Nowicka et al., 2019). Filtering was applied to cells using the following settings 1) FSC-A $\geq$ 5e5 and $\leq$ 4e6 and SSC-A $\geq$ 1e5 and $\leq$4e6; 2) 0.75 $\leq$ Ratio of FSC-H:FSC-A $\geq$ 1.25; 3) FSC-H and FSC-A $\leq$ 2e6; 4) Zombie $\leq$ 2.1. Dimensional reduction was performed using *runDR()* function with the input of up to 5e3 cells per sample without using forward scatter, side scatter, or mtD2 as inputs. Clustering was performed using bluster (v1.0.0) R package on the UMAP embeddings of the SingleCellExperiment object, with mtD2 excluded as an embedding variable. The clustering involved a two-step approach of k-means clustering with centers equal to 1,000 and a nearest neighbor approach using the igraph walktrap function. Clusters identified two doublet/multiplet clusters with the expression of $\geq$ 2 lineage markers, which were manually removed. NK and T cells were separated manually by the expression of NK1.1 and TCRb. MtD2 positivity was defined as transformed values of $\geq$ 1.5. Secondary panel cluster assignments were performed by first correcting between panel variability using the common fluorescent markers of both panels. The correction utilized the mutual nearest neighbor (MNN) approach using k = 50 in the *fastMNN()* function from the batchelor (v1.8.1) R package (Haghverdi et al., 2018). The corrected values were then used to calculate approximate nearest neighbors for each cell using the RANN (v2.6.1) R package. Of the 50 approximate nearest neighbors calculated, a cluster was assigned to an individual cell if 35 or more of these neighbors were from a single cluster.

Detection of cell-free mitochondria in whole blood and plasma

For detection of adipocyte-derived mitochondria in whole blood, 10-20 μL blood was obtained from the tail vein and anti-coagulated in 230-240 μL PBS containing 1 mg/mL heparin sodium salt (Grade I-A, >180 USP units/mg, Sigma-Aldrich, catalog number H3149-1MU) and held on ice till processing. Cellular components were pelleted by centrifugation at 500 x *g* for 5 min at 4°C, and 200 μL of the supernatant was collected for flow cytometric analysis on an Aurora spectral flow cytometer (Cytek Biosciences). The FSC voltage was set to 675 mV (cells are collected at 20 mV for peritoneal lavage cells and BV2 cells or 50 mV for adipose tissue cell preparations), and events were visualized in SpectroFlo 2.0 software (Cytek Biosciences) with FSC-A and SSC-A on log scale. Flow Cytometry Sub-Micron Size Reference Kit beads (Invitrogen, catalog number F13839, lot 1912704) with diameters of 2.0, 1.0, or 0.5 μm were used to verify particle sizes. mtD2+ events were identified in SpectroFlo 2.0 or FlowJo v11 software. The Aurora was programmed to acquire events from 100 μL of the 200 μL sample. Adipocyte-derived mitochondria per mL whole blood were determined by correcting for dilution factors and acquisition volumes.

For detection of cell-free mitochondria in plasma, 250-500 μL blood was obtained from the inferior vena cava or retroorbital sinus and anticoagulated with 10 μL of PBS containing 50 mg/mL heparin sodium salt). Blood was held on ice until processing. The cellular fraction was pelleted by centrifugation at 500 x *g* for 5 min at 4°C, and 50-150 μL cell-free plasma was collected. The plasma was centrifuged at 15,000 x *g* for 5 min at 4°C to pellet mitochondria. The 15,000 x *g* pellet was resuspended in 50 μL of FACS buffer containing 5 μg/mL FcBlock, rat anti-mouse CD41-BV421 (BioLegend, catalog number 133911, clone MWReg30, 1:200), rat anti-mouse TER-119-PB (BioLegend, catalog number 116231, clone TER-119 1:200), rat anti-mouse CD45-PerCP/Cy5.5 (BioLegend, catalog number 103131, clone 30-F11, 1:200), Armenian hamster anti-mouse CD81-PE (BioLegend, catalog number 104905, clone Eat-2, 1:200), rat anti-mouse CD63-PE/Cy7 (BioLegend, catalog number 143909, clone NVG-2, 1:200), and rat anti-mouse CD9-APC (BioLegend, catalog number 124812, clone MZ3, 1:200) and incubated on ice for 30 min. The particles were washed with 1 mL FACS Buffer and centrifuged at 15,000 x *g* for 5 min at 4°C, and the pellet was resuspended in 400 μL FACS Buffer. The Aurora was programmed to acquire 200 μL of the 400 μL sample, and adipocyte-derived mitochondria were defined as mtD2+ events. Adipocyte-derived mitochondria per mL plasma were determined by correcting for dilution factors and acquisition volumes.

For detection of TOM22+ adipocyte-derived mitochondria in plasma, we obtained 600-700 μL blood via cardiocentesis from MitoFat mice. As described above, we collected 200 μL plasma, added 1 mL 1X Separation Buffer and 50 μL anti-TOM22 microbeads (both from Miltenyibiotec's Mitochondria Isolation Kit, Mouse Tissue) in 1.5 mL tubes. Samples were covered in foil and incubated at 4°C for 1 hour with continuous rocking. The specimens were passed over pre-wet LS Columns (Miltenyibiotec) in QuadroMACS magnets (Miltenyibiotec) and washed 3 times with 0.5 mL 1X Separation Buffer, with collection of the wash effluent (non-magnetic fraction). The magnetic particles were eluted from detached LS columns with 1.5 mL 1X Separation Buffer. The magnetic and

non-magnetic fractions were centrifuged at 15,000 x *g* 4°C for 5 min, and the supernatants were discarded. The pellets were resuspended in 100 μL FACS Buffer containing anti-CD41-BV421 (1:200), anti-TER-119-PB (1:200), and anti-CD45-PerCP/Cy5.5 (1:200) with 5 μg/mL FcBlock. After a 30 min incubation on ice, 1 mL FACS Buffer was added, and the specimens were centrifuged at 15,000 x *g* at 4°C for 5 min. The pellets were resuspended in 400 μL FACS Buffer, and 200 μL was acquired on an Aurora flow cytometer. CD41- TER-119- CD45- mtD2+ events were counted to determine the proportion of TOM22+ and TOM22- adipocyte-derived mitochondria in plasma.

Clodronate liposome depletion of macrophages

Female MitoFat mice were treated two times per day (10:00 AM and 5:00 PM) for 2 consecutive days with 150 μL Control Liposomes for Clophosome (Neutral; FormuMax Scientific Inc., Sunnyvale, CA, catalog number F70101-N, batch 11032001) or 150 μL Clophosome Clodronate Liposomes (Neutral; FormuMax Scientific, catalog number F70101C-N, batch 10052101-1019) per injection. Blood was collected from the tail vein at 9:00 AM on Days 0 (before treatment), 1, and 2 to quantify adipocyte-derived mitochondria in blood. On Day 2, oWAT was harvested to confirm macrophage depletion, as described above.

Histologic analyses of adipose and heart

eWAT, iWAT, and BAT were fixed in 4% paraformaldehyde (PFA) in PBS (Santa Cruz Biotechnology, Dallas, TX, catalog number sc-281692) at 4°C for at least 48 hours. Tissues were washed in PBS and submerged and submitted to the WashU Musculoskeletal Research Center Morphology Core for embedding in paraffin blocks, sectioning, and hematoxylin and eosin (H&E) staining. Unstained sections were dewaxed in xylene, rehydrated with gradient ethanol, and then subjected to heat-induced antigen retrieval in citrate buffer (Sigmal-Aldrich, catalog number C9999) using a 2100 Retriever (Electron Microscopy Sciences, catalog number 62706). After quenching of endogenous peroxidase with BLOXALL Endogenous Enzyme Blocking Solution (Vector Laboratories, catalog number SP-6000), sections were stained by immunohistochemistry (IHC) using an anti-mouse Cleaved Caspase-3 antibody (1:1,000, Clone 5A1E, Cell Signaling Technology, catalog number 9664) and the ImmPRESS HRP Universal (Horse Anti-Mouse/Rabbit IgG) PLUS Polymer Kit (Vector Laboratories, catalog number MP-7800). Slides were counterstained with hematoxylin (Vector Laboratories, catalog number H-3401). H&E and IHC images were obtained with an Echo Rebel brightfield microscope (Discover ECHO, San Diego, CA) configured with a 10X flip-out Achromat condenser. Images were obtained with a 40X Apochromat N.A. 0.95 objective. To detect $CD31^+$ vessels in eWAT, iWAT, and BAT, unstained tissue sections were prepared as described above and then stained with goat anti-mouse CD31/PECAM antibody (2 μg/mL, R&D Systems, catalog number AF3628) overnight at 4°C followed by three washes with Tris-Buffered Saline (TBS). Secondary stain with Alexa Fluor 594 AffiniPure Donkey Anti-Goat IgG (0.25 mg/mL, Jackson ImmunoResearch, catalog number 705-585-147) was performed at room temperature for 45 min. After three washes in TBS, the slides were mounted with 20 μL Flouromount-G with DAPI (Invitrogen, catalog number 00-4959-52). Images were obtained on a Lionheart FX fluorescent microscope (Agilent Technologies, Santa Clara, CA) with a 4X objective.

For histology analysis of the heart, MitoFat mice were perfused with ~30 mL ice-cold PBS via the inferior vena cava (IVC) using a Fisherbrand Variable-Flow Peristaltic Pump (Fisher Scientific, catalog number 13-876-2). Ventricles were dissected and placed in 4% PFA at 4°C. After fixation, hearts were rinsed with PBS x 3 and infiltrated with 30% sucrose (in PBS) overnight at 4°C. Hearts were embedded in O.C.T. (Fisher HealthCare Tissue Plus O.C.T. Compound Cat 4585) and frozen at -80°C. 30 μm sections were obtained using a Leica Cryostat. Sections were then washed in TBS. DAPI mounting, anti-fade solution (Vectashield Cat #H-1200) was added immediately prior to placement of no. 1.5 coverslips. Images were obtained with Zeiss LSM 700 confocal microscope installed on an AxioImager.M2. Acquired images were processed using ZEN Blue and/or Black. Heart sections were imaged with a 40X objective lens using z-stack features. The observer was blind to genotype and diet group.

Fatty acid (FA)-conjugation to bovine serum albumin (BSA)

FA-BSA stocks were prepared fresh prior to each experiment using the following fatty acids: lauric, myristic, palmitic, stearic, oleic, and linoleic acids (all from Sigma-Aldrich). To facilitate solubilization, 80 mM of each FA was saponified in 0.1 M aqueous KOH or NaOH with heating to 70 °C and constant agitation using an Eppendorf ThermoMixer. Utilizing established binding parameters (Table S3), saponified FAs were added to pre-warmed (37°C) 2 mM FA-free BSA (Roche) in PBS to achieve unbound free fatty acid concentrations equal to 11.03 nM. This concentration was selected because 0.5 mM palmitate conjugated to 0.125 mM BSA (4:1 ratio) is commonly used and equates to 11.03 nM unbound FFA, assuming a dissociation constant (K_d) of 8 nM and 6.9 predicted palmitate binding sites per molecule of BSA (Huber et al., 2006). The K_d values and number of predicted binding sites for each fatty acid are shown in Table S3. Conjugation was carried out in an orbital shaker (New Brunswick), rotating at 140 rpm at 37 °C for 1 hr. Conjugates were filter-sterilized through 0.2 μm PVDF filters and added to fresh cell culture media.

BV2 cell culture

Culturing of BV2 cells was described previously (Brestoff et al., 2021). In brief, BV2 cells were maintained in "BV2 Media" which consisted of high glucose DMEM containing 10% heat-inactivated FBS (Corning or Gibco) supplemented with penicillin, streptomycin, and L-glutamine. For the indicated amounts of time (0.5, 4, or 24 hours) prior to harvest, BV2 cells were treated with BSA or BSA-fatty acid conjugates. BV2 cells were then washed once in sterile PBS and incubated with 0.05% trypsin-0.44 mM EDTA in DPBS (Gibco) for 5 min at room temperature. The cells were collected and counted using a Countess II (Invitrogen), and 5×10^4 live cells were plated in each assay well (96 well round-bottom plate from MidSci or Corning) for immediate use in the mitochondria uptake assay described

below. In some experiments, we made BV2 media with DMEM without glucose (Corning, catalog number 17-207-CV), and then glucose (>99.5%, Sigma, catalog number G8270-1KG, lot #SLCD0829) or sucrose (BioXtra, >99.5%, Sigma, catalog number S7903, lot #SLCK8454) was added to the media at low (5.55 mM) or high (25 mM) concentrations. Adherent BV2 cells were cultured with low glucose, high glucose, low sucrose, or high sucrose BV2 Media for 24 hours prior to use.

Generation of bone marrow-derived macrophages (BMDMs)

Bone marrow was harvested from femurs and tibias of *Cd36*$^{+/+}$ or *Cd36*$^{-/-}$ mice (n=4 each) as previously described (Amend et al., 2016). Marrow suspensions from each set of long bones (1 tibia and 1 femur) were passed through 100 μm Nylon strainers and seeded on 2 x 150 mm non-TC-treated dishes in "D10 Media," which is comprised of high glucose DMEM (Corning) containing 10% heat-inactivated FBS (Corning) supplemented with 1x penicillin-streptomycin (Corning) and 10% CMG14-12 supernatant (contains 1.3 μg/mL M-CSF, a generous gift from Dr. Steven L. Teitelbaum). Cells were cultured for 7 days at 37°C with 5% CO_2, with fresh D10 Media applied every 2-3 days. On day 7, cells were washed once in 37 °C PBS and lifted by incubating with 0.25% Trypsin/2.21 mM EDTA (Corning) for 5 minutes at 37 °C and counted as described above (under "BV2 cell culture"). A total of 1.2 x 10^6 cells were seeded in D10 Media on 100 mm non-TC-treated dishes and allowed to adhere overnight prior to treatment with the BSA-conjugated fatty acids or BSA alone in D10 Media for 24 hours. Cells were then lifted with ice-cold 5 mM EDTA in PBS (Sigma), counted, and 5 x 10^4 live cells were dispensed in round-bottom 96 well round-bottom assay plates (Corning or MidSci) for immediate use in the mitochondria uptake assay described below.

Isolation of purified mitochondria

mtD2 global mitochondria reporter mice or *Ndufs4*$^{+/+}$ or *Ndufs4*$^{-/-}$ mice were euthanized and livers were perfused with 10 mL sterile PBS via the left ventricle. About 0.5-1.0 grams of liver were harvested and minced finely on a dish held on ice. The liver was homogenized in 1 mL ice-cold lysis buffer from the Miltenyi Biotec Mitochondria Isolation from Mouse Tissue Kit supplemented with 1X (1:100) Halt Protease/Phosphatase Inhibitor Cocktail (Pierce), with 8 passes in a 1mL glass dounce homogenizer (Sigma-Aldrich). The homogenate was brought to 10 mL with 1X separation buffer and mixed by inversion, and 50 μL of anti-TOM22 microbeads were added. The samples were wrapped in foil and incubated on a rocker at 4 °C for 1 hour. Cellular debris was pelleted with a pulse centrifugation at 500 x *g* at 4 °C for 1 second, and the supernatants were applied to LS columns previously wetted with 1X separation buffer (ice cold). The columns were washed 3 times each with 2 mL ice-cold 1X separation buffer before elution with 1.5 mL 1X Separation Buffer. Isolated mitochondria were pelleted by centrifugation at 13,000 x *g* at 4 °C for 2 min. The supernatants were discarded, and the mitochondria were resuspended in 1.0 mL Storage Buffer (Miltenyi Biotec) and held on ice. Mitochondrial protein concentration was measured using the Coomassie Plus Protein Assay Reagent (Thermo Scientific, catalog number 1856210) with absorbance at 595 nm and a BSA (Pierce) standard curve.

Mitochondria uptake assay

Aliquoted BV2 cells or BMDMs (5 x 10^4/well) were centrifuged at 500 x g for 5 min at 4 °C and then resuspended in BV2 Media with or without 10 μg/mL mtD2 mitochondria (in 200 μL). Cells exposed to mitochondria isolates were incubated at 37 °C with 5% CO_2 for 1 hour. Cells were centrifuged at 500 x g for 5 min at 4 °C, washed once with 200 μL PBS, and then resuspended in 50 μL PBS containing 1:1,000 Zombie-NIR and incubated on ice for 5 min. The stain was quenched with 200 μL FACS Buffer. Cells were centrifuged as described above and washed twice more in 200 μL FACS Buffer before being acquired on a Cytek Aurora spectral flow cytometer. Cells were pre-gated on singlet, live cells before determining the percent of mtD2+ cells and the mean fluorescence intensity (MFI) for mtD2 (within mtD2+ cells) using FlowJo v10.0 analytic software.

Administration of purified mitochondria to mice and isolation of peritoneal macrophages

Purified mtD2 mitochondria were isolated from livers as described above, and 500 μg/mL mitochondria in ice-cold PBS were prepared. Purified mitochondria (200 μL to deliver 100 μg/mouse) or PBS (200 μL) were administered by intraperitoneal injection once to either *Ndufs4*$^{+/+}$ or *Ndufs4*$^{-/-}$ mice. Peritoneal lavage cells were harvested 1, 2, or 3 days later for flow cytometric analysis of mtD2 mitochondria uptake by live CD45$^+$ F4/80$^+$ CD11b$^+$ peritoneal macrophages. On Day 1, peritoneal macrophages were purified using magnet-associated cell separation (MACS) using anti-F4/80 MicroBeads UltraPure (Miltenyi Biotec, catalog number 130-110-443) using QuadroMACS magnets (Miltenyi Biotec, catalog number 130-090-976) and LS Columns (Miltenyi Biotec, catalog number 130-042-401), according to manufacturer instructions. Purity was confirmed to be >95% by flow cytometry.

Seahorse mitochondrial stress test assays

Purified peritoneal macrophages (3 x 10^4) or oWAT macrophages (5 x 10^4) were plated onto 8-well Agilent Seahorse XF HS PDL Miniplates (Agilent Technologies), which contain plastic rings that consolidate cells at higher density in the center of the well. After adherence for 1 hour (peritoneal macrophages) or 2 hours (oWAT macrophages) at 37°C in Phenol-free XF DMEM supplemented with 1 mM Pyruvate, 2 mM Glutamine, and 10 mM Glucose, cells were analyzed using Agilent Seahorse XF Cell Mitochondria Stress Test Kits on an Agilent Seahorse XF HS Mini machine. FCCP concentrations were optimal at 2 μM for peritoneal macrophages and oWAT macrophages, and oligomycin was used at 1.5 μM, antimycin A at 0.5 μM, and rotenone at 0.5 μM.

For BV2 cells, 1.5 x 10^6 cells were plated on 100 mm dishes and allowed to adhere overnight before being treated for 30 min with 1 μM Rotenone in DMSO plus 1 μM Antimycin A in 100% ethanol (R+A) or DMSO:ethanol vehicle as a control. Cells were washed and

lifted with 0.05% trypsin-EDTA in PBS and then counted with a Countess FL with 0.1% trypan blue. 5 x 10^4 cells were plated into each well of a 96-well round-bottom plates (tissue culture-treated) for exposure to 10 μg/mL purified liver mitochondria from *Ndufs4*$^{+/+}$ or *Ndufs4*$^{-/-}$ mice. Cells were cultured with purified mitochondria for 1 hour at 37°C with 5% CO_2. Cells were then centrifuged at 500 x *g* for 5 min at 4°C, washed twice with 200 μL BV2 media to remove extracellular mitochondria, and then counted again with a Countess FL with 0.1% trypan blue. XF96 Microplates were coated with Poly-D-Lysine (PDL) at 50 μg/mL (Gibco, catalog number A38904-01) in sterile DPBS for 1 hour at room temperature followed by 3 rinses with sterile water and air drying in a laminar hood for 2 hours before use. Cells were seeded at 1 x 10^4 cells per well in PDL-coated Microplates in Phenol-free XF DMEM supplemented with 1 mM Pyruvate, 2 mM Glutamine, and 10 mM Glucose and allowed to adhere for 1.5 hours in a non-CO_2 incubator at 37°C. Extracellular Flux Assay Kits were used to perform Mitochondria Stress Test Assays on a 96-well XFe Seahorse analyzer (Agilent) according to manufacturer protocols. FCCP concentrations were optimal at 2 μM for BV2 cells, and oligomycin was used at 1.5 μM antimycin A at 0.5 μM, and rotenone at 0.5 μM.

After the assay was completed, brightfield imaging was done with an Agilent Cytation 5 with a 4X objective (96 well plate) or an Echo Rebel inverted microscope with a 10X objective (8 well plate with ring). ImageJ was used to calculate the number of adherent cells per well. Seahorse data were analyzed in Seahorse Analytics software (Agilent). For BV2 cells and peritoneal macrophages, the data were normalized by dividing oxygen consumption rates (OCR) by the ratio of adherent to input cell counts. For oWAT macrophages, the cell seeding pattern precluded reliable cell counting with ImageJ, therefore for this cell type we visually confirmed similar cell densities across wells after the Seahorse assays and analyzed raw OCR values per Agilent recommendations.

Statistics

Analyses was performed in R v4.0.2 and Prism v9 (Graphpad, La Jolla, CA). Categorical data was processed using the dplyr (v1.0.2) and tidyr (v1.1.2) R packages with visualizations using the ggplot2 (v3.3.2), ggthemes (v4.2.0), viridis (v0.5.1) R packages. Student's t-tests were performed for 2-group comparisons, one-way analysis of variance (ANOVA) with Dunnet or Tukey post-hoc testing was used for three-or-more group comparisons, and 2-way ANOVA with Sidak or LSD posthoc testing was used for 2 x 2 designs. Paired testing or repeated measures was used when appropriate. When the standard deviations between groups differed, the appropriate correction was applied (e.g. Welch's correction). Statistical significance was set at $P<0.05$.